ISSN 0735-1348

Ancient TL

A periodical devoted to Luminescence and ESR dating

Department of Physics, East Carolina University, 1000 East 5th Street, Greenville, NC 27858, USA
http://www.ecu.edu/cs-cas/physics/ancient-timeline/

June 2016, Volume 34 No.1

External beta dose rates to mineral grains in shell-rich sediment 1
Alastair C. Cunningham

Source and characteristics of blue, infrared (IR), and post-IR IR stimulated signals from gypsum-rich samples 6
Laine Clark-Balzan

Sources of variability in single grain dose recovery experiments: Insights from Moroccan and Australian samples 14
Nina Doerschner, Marion Hernandez and Kathryn E. Fitzsimmons

Thesis abstracts 26

Bibliography 32

Announcements 42

Ancient TL

Started by the late David Zimmerman in 1977

Ancient TL

External beta dose rates to mineral grains in shell-rich sediment

Alastair C. Cunningham[1]*

[1]Centre for Archaeological Science, School of Earth and Environmental Sciences, University of Wollongong, Wollongong, NSW, Australia

*Corresponding Author: acunning@uow.edu.au

Received: December 17, 2015; in final form: April 11, 2016

Abstract

Luminescence dating methods make use of the infinite-matrix assumption to simplify dose rate calculations. This works well when the sediment grain size is much smaller than the range of beta electrons in sediment (∼3 mm). However, shell material introduces complexity in the beta dose rate calculations, because it creates low-dose-rate zones where no mineral grains are present. This phenomenon introduces an error in the estimated beta dose rate, whether or not the shells are included in the beta dose-rate measurements. The magnitude of the error depends on the size and shape of the shell material, and the quantity of it. Here, this relationship is modelled using Monte Carlo radiation transport software. The model indicates that for shell masses below 25 %, accurate estimates of beta dose rate are readily obtained from: 1) the infinite matrix dose rate of the bulk material (including shells) when shell fragments are small ($< \sim$0.001 cm^3); and 2) the infinite matrix dose rate of the sandy fraction (without shells) when shell fragments are larger ($> \sim$1 cm^3). Between these extremes of shell size, e.g. for shell-hash samples, a significant correction to the measured beta dose rate is necessary.

Keywords: luminescence, shell, carbonate, dose rate

1. Introduction

Shell material can make up a significant proportion of some types of coastal sediment. While fine shell fragments ($\sim$0.001 cm^3) are often present in coastal dunes, larger shell fragments ($\sim$0.03 cm^3) can be concentrated in shell hash, forming a major part of coastal barrier sequences. Beds of whole valves and articulated shells can be laid by storm surges or tsunamis, and large concentrations of shells can be found in middens.

Optically Stimulated Luminescence (OSL) methods generally work very well for coastal sediment, but dating the shell-rich deposits presents an additional complication for the beta dose-rate calculations. The complexity arises because shell material makes the sediment non-uniform at the range of beta electrons, so invalidating the infinite-matrix assumption. As a consequence, the dose received by the dosimeter grains is less than the infinite-matrix dose (Nathan et al., 2003). While it is often possible to avoid shell-rich beds by sampling the bracketing horizons (e.g. Bateman et al., 2008), it may be necessary or desirable to target the shell-rich beds directly (e.g. Cunningham et al., 2011; Pluckhahn et al., 2015). For such sediments, OSL does have advantages over other dating methods, provided the dose-rate complications are surmounted. Radiocarbon dating and amino-acid racemization can be applied to shell material, but can be erroneous if the shell ages are not contemporary with the deposition event. For example, Oliver et al. (2015) dated a Holocene barrier sequence with quartz OSL (targeting aeolian sand beds), and found a significant offset from a previous chronology which used radiocarbon on shell hash. Radiocarbon ages of marine shells also require a reservoir correction, and terrestrial shells are problematic due to hard-water effects.

For shell-rich sediment, the disparity between the actual and infinite-matrix dose rates depends on the size and quantity of shell material. The effect can be modelled using a Monte Carlo radiation transport code, once estimates have been made of the shell size and quantity, and the radionuclide concentrations. This was done by Cunningham et al.

(2011) for a shell-rich storm-surge bed and a shell hash sample, with the OSL ages, once corrected, neatly matching the bracketing OSL dates on aeolian sand. However, such an undertaking may not be justified unless it is known that a large dose-rate correction needs to be made. If the shell content is low enough, or the shells are small enough, then the error resulting from the infinite-matrix assumption will be tolerable.

The purpose of this paper is to assess how the beta dose rate to quartz grains is influenced by the size and quantity of shell material. It is intended to help readers decide what strategy to use for beta dose-rate measurements when shells are present, and whether further modelling would be beneficial for their samples. The phenomenon of interest also affects the external beta dose to feldspar grains. However, unlike quartz grains, feldspar grains also have a significant internal beta dose, so the consequence of an error in the external beta dose rate is less severe. It is assumed here that the shell material is discrete and its composition constant over time. Complications arising from carbonate cementation and uranium uptake are discussed elsewhere (Zander et al., 2007; Nathan & Mauz, 2008).

2. The phenomenon

Typically, beta dose rate estimates follow either spectrometry or beta-counting measurements. In both cases, the sample is homogenised before measurement and the infinite-matrix (IM) assumption is used, i.e. the rate of radiation absorption is presumed equal to the rate of radiation emission (Aitken, 1985). The distribution of radionuclides is also presumed to be uniform. For sandy or silty sediments this assumption is reasonable because the range of beta particles ($\sim$3 mm) is much larger than the diameter of the grains (although see Guérin et al., 2012).

The introduction of shell material to the sediment creates non-uniformity in the beta field. The sediment now contains two different zones: the solid shell, and the sand matrix. Shell consists of calcite or aragonite with a density of $\sim$2.70 g cm^{-3}. Although the density of the shell is comparable to minerals in the sand matrix, the shell does not contain any pore space. The shell material is therefore more efficient at absorbing radiation per unit volume compared to the sand matrix (mean density $\sim$1.80 g cm^{-3}). In addition, shell material has an extremely low radionuclide concentration, providing an infinite-matrix beta dose rate of $\sim$0.02 Gy ka^{-1}. Beta dose rates provided by the sand matrix depend on the mineralogical composition, but would typically be at least an order of magnitude larger: beta dose rates of 0.50 - 1.00 Gy ka^{-1} are typical for coastal settings (e.g. van Heteren et al., 2000; Ballarini et al., 2003).

The presence of the shell material creates zones in the sediment with low beta dose rates. The dosimeter grains, be they quartz or feldspar, are excluded from this zone, so are not subject to the lowest beta dose rates possible in the bulk sediment. The exclusion of the dosimeter grains from low-dose regions means the actual dose rate to the sand matrix is higher than the infinite-matrix dose rate. However, the dose rate in the sand matrix is also affected by proximity to the shells: grains closer than $\sim$3 mm to a shell have a dose rate lower than the remainder of the sand matrix, because the shell is not emitting as much beta radiation as it absorbs.

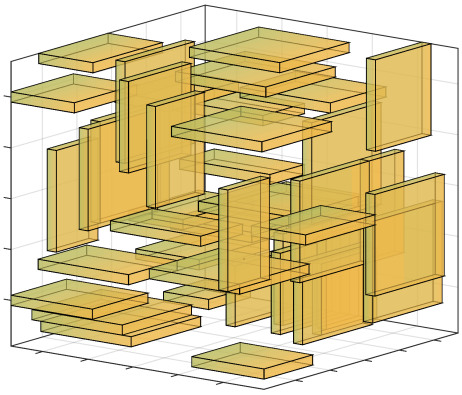

Figure 1. Example of the dimensionless model geometry. Rectangular cuboids representing the shells are added in one of the two orientations until the desired mass fraction is reached (20 % in this case). Shells may not overlap, but may lie adjacent to one another.

This phenomenon presents a conundrum for dose rate estimation. If a shell-rich sample is homogenised before spectrometry or beta-counting measurements, then the beta dose rate to the dosimeter grains will be underestimated. However, if the shells are removed before homogenisation, then the dose rate will be overestimated because of the proximity effect. The actual beta dose rate to the grains must lie between these extremes (the bulk-sample IM dose rate, and the sand-matrix-only IM dose rate; hereafter 'bulk-IM' and 'sand-IM'), and will depend on the size and quantity of the shells.

3. Monte Carlo Modelling

Monte Carlo radiation transport software simulates particle interaction in a specified geometry, with the option of recording the energy deposited in particular regions. This study uses the MCNP4C software (Briesmeister, 2000) and a simple, cellular geometry. A brief description of the model set-up is given here; full details, including sensitivity tests, are provided in the supplementary files of Cunningham et al. (2011).

The model geometry is constructed by randomly placing rectangular cuboids within a larger cube (Fig. 1). The cuboids have relative dimensions 10 : 10 : 1. The cuboids represent shells or shell fragments; they are placed in one of two orientations, until the desired volume fraction is filled with 'shells'. The shells are given a material of $CaCO_3$, density 2.70 g cm^{-3}. The remaining space is defined with a material combination of SiO_2 and H_2O and represents the sand matrix with density 1.82 g cm^{-3}, reflecting a water content of 5 % and packing density of 65 %.

Each shell, and the sand matrix, is defined as a source region for beta particles. The beta energy spectra for the sand and shell source regions are different. The spectra were generated by Cunningham et al. (2011) using gamma-spectrometry derived radionuclide concentrations for both sand and shell, which were used to weight the beta energy spectra for K, and the U and Th chains. There is a 28 : 1 ratio of energy emitted per unit mass between sand and shell. These spectra were designed for a particular coastal sample from North Holland; their use here in a generalised model is reasonable in my view, as differences in the radioactivity from sample to sample will not affect the order-of-magnitude difference between the two components.

The model has a single dosimeter, the sand-matrix region, in which the deposited energy is recorded. Particles hitting the boundary of the geometry are reflected back in random directions to maintain charged-particle equilibrium. Five different geometries were constructed with shell mass fractions of 5 %, 10 %, 20 %, 30 % and 40 %. Different shell sizes were simulated by changing the dimensions of the geometry, effectively changing the volumes of the individual shells. Each of the five geometries was used for 10 different shell volumes between 0.0001 cm^3 and 2.70 cm^3, resulting in 50 variations of the simulation.

4. Results

The simulation output consists of energy deposited in the sand matrix (where the dosimeter grains must be located), through the interaction of beta electrons and their secondary particles. In Fig. 2, these values are expressed as a proportion of the bulk-IM and sand-IM beta doses. Fig. 2a shows the ratio of the modelled dose to the bulk-IM dose, as a function of individual shell volume and total shell mass. The biggest departure from the bulk-IM dose occurs where shells are large and numerous. As the shell size and quantity becomes smaller, the modelled beta dose approaches the bulk-IM dose.

Fig. 2b shows the same model output, expressed as a proportion of the sand-only IM dose. When there are a small number of larger shells, the modelled dose to the sand matrix is similar to its IM dose; when there are a large number of small shell fragments, the modelled dose is much smaller than sand-IM dose.

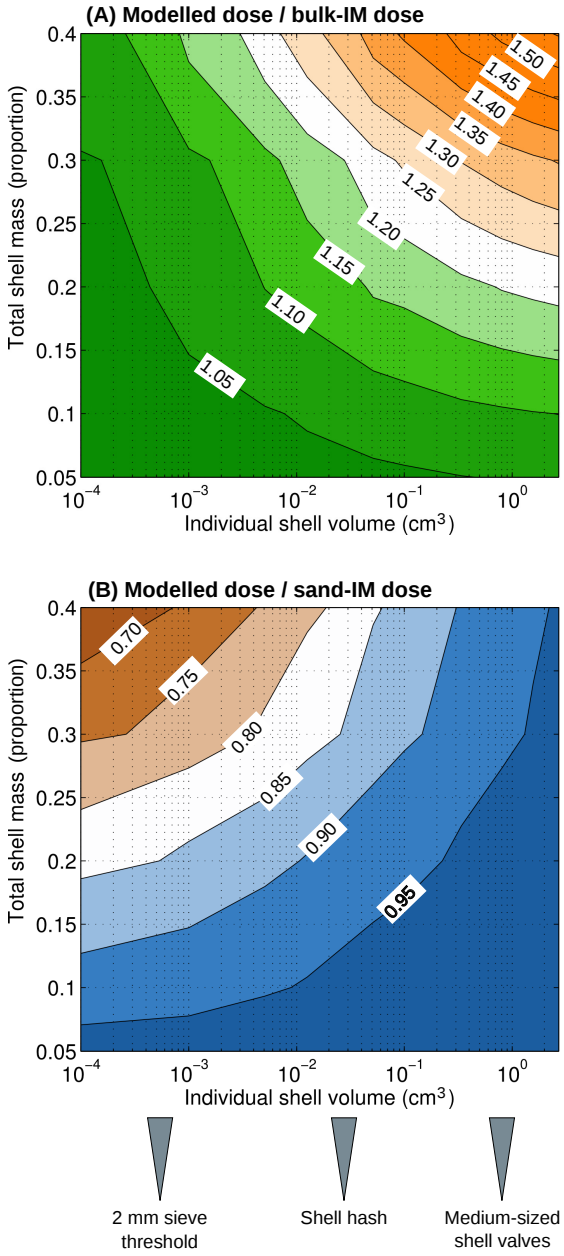

Figure 2. Results of Monte Carlo transport simulations. (a) Contour map showing the ratio of the dose received by the sand matrix to the bulk-sample infinite matrix (IM) dose, as a function of the individual shell volume and the total shell mass. (b) Contour map showing the ratio of the dose received by the sand matrix to the sand-IM dose, as a function of the individual shell volume and the total shell mass. Also indicated are the approximate volumes of medium-sized shell valves, shell hash, and the fragments around the 2 mm sieve threshold.

5. Discussion

The model used here makes use of some simplifications in geometry, making the analysis easier but more limited in scope. The first limitation comes through the use of voxelisation: the shells must be placed on a discrete coordinate system. When packed densely, the shells are liable to stack on top of each other, with no intervening space for the sand matrix. This is a poor simulation of the natural sediment, where even closely packed shells are likely to have some sand grains in between. Assessed visually, the model geometry is susceptible to this effect at shell mass fractions greater than 30 % (and is responsible for the kink in the contour plots for the 30 % shell-mass simulations). The second limitation lies in the choice of shell dimensions. The dimension ratio 10 : 10 : 1 was used to approximate a medium-sized shell with length and width of 2 cm, and thickness 0.2 cm, and this ratio was kept constant for smaller shell volumes. This is not very realistic for fine shell fragments, which in nature

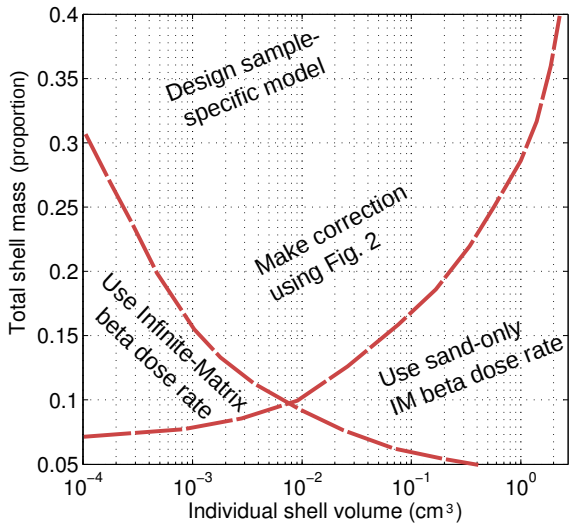

Figure 3. Visual decision guide to help choose a measurement strategy for the beta dose, as a function of the shell mass fraction and the size of the shells. Lines indicate the suggested threshold of 5 % error in beta dose rate.

are likely to be less elongated. With these two known limitations, the model is most robust for the bottom right of the contour plots (Fig. 2), and least robust for the top left. In a further limitation, it is assumed all shells within a simulation run are the same size. While this is obviously a simplification, sorting does occur in fluvial and aeolian sedimentation, as it does in shell midden formation, and it is the order-of-magnitude differences in shell size that are of concern here.

In designing a decision strategy for samples with shell material, it should be noted that the external beta dose to quartz grains contributes ∼60 % of the annual dose. For feldspar, the relative contribution of external beta dose will be lower (< ∼50 %) due to an additional component of internal beta radiation. An error of 5 % in the external beta dose rate therefore equates to ∼3 % error in the total dose rate and age estimate for quartz, and < 2.5 % for feldspar. Given the other sources of uncertainty in OSL dating, a 3 % error in the age can usually be tolerated. A decision strategy can then ascertain whether this tolerance is exceeded. The strategy can be demonstrated by considering shell material of three different sizes, each indicated on Fig. 2:

1. *Medium to large shells (volume per shell >∼1 cm^3).* If the pieces of shell material are relatively large, then the beta dose to the sand is similar to the sand-IM dose. With reference to Fig. 2b, a mass fraction of medium to large shells of up to 30 % will result in a tolerable error in the beta dose of under 5 %, provided that the beta dose measurements are performed on the sand fraction.

2. *Fine shell fragments (volume per fragment <∼0.001 cm^3).* Fine shell fragments have little effect on the bulk-IM dose rate. The error on the bulk-IM dose rate is tolerable for a mass fraction up to ∼25 %. In most cases therefore, fine shell fragments can be included in beta dose measurements.

3. *Shell hash.* Shell material with the size range of shell hash presents a problem. If the total shell mass is > 10 %, both the bulk-IM dose rate and the sand-only IM dose rate result in a significant error. For example, a shell-hash mass fraction of 30 % will create ∼20 % error in the beta dose rate, whether or not the shells are included in the beta-dose measurements. A correction will be then be required.

Figure 3 shows a graphical visualisation of this decision strategy. Required beforehand are the mass fraction of the shell material (i.e. mass of the >1 mm fraction, divided by the total sediment mass), and the approximate volume of the individual shell fragments (e.g. A × B × C axes of a fragment, or its mass in grams divided by 2.71). If the shell material is large or very fine, then the resulting strategy is straightforward. Shell fragments of the size found in shell hash will demand a correction be applied to the dose rate. A rough correction could be made using Fig. 2a or Fig. 2b; a more precise correction would require a sample-specific Monte Carlo model.

6. Conclusion

Discrete shells or shell fragments in sediment create an error in the beta dose rate estimate to quartz or feldspar grains used as dosimeters. This error occurs whether or not the shells are included in the homogenised measurements for beta dose-rate assessment. If shells are medium-sized or larger (>∼1 cm^3), the error is probably tolerable if they are removed from the sample before homogenisation. Fine shell fragments (passing 2 mm sieve) can usually be homogenised with the bulk sample. If small shells or shell-hash sized fragments are present at a mass fraction of >10 %, the beta dose rate will need to be corrected.

If shell material is present, it is straightforward to record its total mass and the approximate size of the shells. With this information, the decision strategy in this paper can be used. In most cases a tolerable error can be achieved without need for correction, but in some cases the correction to the beta dose rate will be required. However, even a small correction may be beneficial; for example, variability in the shell content within a set of samples, if uncorrected for, would create additional sample-to-sample scatter in the age.

Acknowledgments

My thanks to Didier Miallier for reviewing the manuscript, and to Jakob Wallinga for commenting on the draft.

References

Aitken, M. J. *Aitken Thermoluminescence Dating*. Academic Press Inc, London ; Orlando, October 1985. ISBN 978-0-12-046381-7.

Ballarini, M., Wallinga, J., Murray, A. S., Van Heteren, S., Oost, A. P., Bos, A. J. J., and Van Eijk, C. W. E. *Optical dating of young coastal dunes on a decadal time scale*. Quaternary Science Reviews, 22(10): 1011–1017, 2003.

Bateman, M. D., Carr, A. S., Murray-Wallace, C. V., Roberts, D. L., and Holmes, P. J. *A dating intercomparison study on Late Stone Age coastal midden deposits, South Africa*. Geoarchaeology, 23 (6): 715–741, November 2008. doi: 10.1002/gea.20243.

Briesmeister, J. F. *MCNP-A General Monte Carlo Code N-Particle Transport Code Version 4C*. LA-13709-M, Los Alamos National Laboratory, 2000.

Cunningham, A. C., Bakker, M. A., van Heteren, S., van der Valk, B., van der Spek, A. J., Schaart, D. R., and Wallinga, J. *Extracting storm-surge data from coastal dunes for improved assessment of flood risk*. Geology, 39(11): 1063–1066, 2011.

Guérin, G., Mercier, N., Nathan, R., Adamiec, G., and Lefrais, Y. *On the use of the infinite matrix assumption and associated concepts: A critical review*. Radiation Measurements, 47(9): 778–785, September 2012. doi: 10.1016/j.radmeas.2012.04.004.

Nathan, R. P. and Mauz, B. *On the dose-rate estimate of carbonate-rich sediments for trapped charge dating*. Radiation Measurements, 43(1): 14–25, January 2008. doi: 10.1016/j.radmeas.2007.12.012.

Nathan, R. P., Thomas, P. J., Jain, M., Murray, A. S., and Rhodes, E. J. *Environmental dose rate heterogeneity of beta radiation and its implications for luminescence dating: Monte Carlo modelling and experimental validation*. Radiation Measurements, 37(4): 305–313, 2003.

Oliver, T. S., Dougherty, A. J., Gliganic, L. A., and Woodroffe, C. D. *Towards more robust chronologies of coastal progradation: Optically stimulated luminescence ages for the coastal plain at Moruya, south-eastern Australia*. The Holocene, 25(3): 536–546, March 2015. doi: 10.1177/0959683614561886.

Pluckhahn, T. J., Hodson, A. D., Rink, W. J., Thompson, V. D., Hendricks, R. R., Doran, G., Farr, G., Cherkinsky, A., and Norman, S. P. *Radiocarbon and luminescence age determinations on Mounds at Crystal River and Roberts Island, Florida, USA*. Geoarchaeology, 30(3): 238–260, 2015.

van Heteren, S., Huntley, D. J., van de Plassche, O., and Lubberts, R. K. *Optical dating of dune sand for the study of sea-level change*. Geology, 28(5): 411–414, 2000.

Zander, A., Degering, D., Preusser, F., Kasper, H. U., and Brckner, H. *Optically stimulated luminescence dating of sublittoral and intertidal sediments from Dubai, UAE: Radioactive disequilibria in the uranium decay series*. Quaternary Geochronology, 2(14): 123–128, 2007. doi: 10.1016/j.quageo.2006.04.003.

Reviewer

Didier Miallier

Ancient TL

Source and characteristics of blue, infrared (IR), and post-IR IR stimulated signals from gypsum-rich samples

Laine Clark-Balzan[1]*

[1] Institute of Earth and Environmental Sciences, Geology, Albert-Ludwigs-Universität
Albertstr. 23-B, Freiburg, 79104, Germany

*Corresponding Author: laine.clark-balzan@geologie.uni-freiburg.de

Received: May 1, 2016; in final form: June 3, 2016

Abstract

Samples collected from gypsiferous deposits in the Nefud Desert, Saudi Arabia, yielded anomalous signals when presumed quartz and feldspar extracts were measured with BSL and $pIRIR_{290}$ SAR protocols, respectively. Subsequent scanning electron microscopy analysis indicated that the majority of extracted coarse grains were gypsum instead of quartz or feldspar. Luminescence signals were detected from gypsum at room or low (50 °C) temperature when stimulated with blue (UV detection: 330, 380 nm) or IR (blue detection) light. No UV (330 nm) emissions were detected with IRSL stimulation. A modified SAR protocol (no preheats) was successful in building saturating exponential growth curves for BSL/UV_{380} and IRSL/blue emissions from gypsum, with acceptable recycling and zero ratios. Luminescence measurement of gypsum with standard protocols used for quartz (BSL/UV_{340} SAR with preheats) and feldspar ($pIRIR_{290}$ with preheats) yielded either negligible or anomalous signals that could be excluded from consideration via typical rejection criteria. Additionally, massive decrease in sensitivity with SAR cycle was found to be indicative of gypsiferous content. Therefore measurement of quartz and feldspar aliquots according to standard procedures should be possible even in gypsum-contaminated samples, though concentration of these minerals via an extra density separation step may be necessary.

Keywords: luminescence, gypsum, sample preparation, rejection criteria

1. Introduction

Gypsum ($CaSO_4 \cdot 2H_2O$) is a moderately soluble evaporite commonly found in arid environments. Precipitate deposits may be classified as primary, forming from a supersaturated brine pool, secondary, precipitating in intrasedimentary spaces (e.g. desert roses), or, perhaps most often, a mixture of the two (Warren, 2006). Unless gypsum has formed within a supersaturated water column, mineral inclusions such as quartz and feldspar grains are very common, and physical separation of the minerals is complex and time-consuming (McLeod et al., 1985). Anhydrite ($CaSO_4$) is a closely related mineral that may form naturally, or it can be produced artificially by heating gypsum and inducing the progressive loss of both water molecules. Loss of water from the crystal structure begins at temperatures as low as ∼363 K (∼90 °C) (Lager et al., 1984).

Various attempts have been made to date gypsum or anhydrite via trapped charge dating techniques, such as electron spin resonance and thermoluminescence (Nambi, 1982; Mathew et al., 2004; Nagar et al., 2010; Aydaş et al., 2011). More recently, O'Connor et al. (2011) have shown that room temperature blue light stimulation (470 ± 30 nm) and infrared stimulation (830 ± 10 nm) of both gypsum and anhydrite yield measurable UV (5 mm Hoya U-340) or blue-violet (1 mm Schott BG-39 and 2.5 mm Corning 7-59) and UV emissions. Detschel & Lepper (2009) also detected BSL/UV and IRSL/UV signals (same stimulation/detection as above) from gypsum at room temperature, but only BSL/UV from anhydrite. The irradiating source in this study, however, was ionizing UV radiation from a deuterium source, therefore it may not be directly comparable. O'Connor et al. (2011) also reported that a modified, room temperature SAR protocol adequately corrected for sensitivity changes and could be used to measure a saturating exponential regeneration curve, how-

ever, signal fading was significant (less than 5 % per decade) for all tested combinations except for IRSL/UV of gypsum. Jain et al. (2006) published measurable signal and growth curves from gypsum and anhydrite (BSL/UV), but noted a sensitivity decrease of nearly an order of magnitude after preheating to 260 °C (held 0 s). Mahan & Kay (2012) attempted to date gypsum from Salt Basin Playa via a BSL/UV SAR protocol with preheats of 180 °C for 10 s and BSL measurement at 125 °C, working on the assumption that the complete transformation into anhydrite did not occur until ca. 180 – 200 °C. They also noted severely decreased signal intensity with preheats greater than this temperature. Standard preheats or raised temperature stimulations seem to have a deleterious effect on the signals measured from gypsum, which is likely linked to dehydration of the crystal structure and eventual conversion to anhydrite. It should be emphasized that the above research has shown anhydrite and gypsum to have distinct signal characteristics (Detschel & Lepper, 2009; Jain et al., 2006) and fading rates (O'Connor et al., 2011).

Samples collected from gypsum-rich environments are likely to comprise mineral mixtures which cannot be completely separated, and the experiments described above suggest that gypsum/anhydrite may produce a measurable emission during standard, elevated temperature OSL/IRSL measurement of quartz or feldspar. Luminescence signal contamination can lead to age underestimation if a proportion of the measured signal fades over geological time scales. It may also lead to incorrect dose rate calculations if radioisotope distribution and attenuation factors are miscalculated or poorly understood. Current rejection criteria, such as the IR depletion ratio (Duller, 2003), ensure that feldspar dominated aliquots are excluded from quartz BSL populations, while IRSL emissions from quartz will be negligible during typical feldspar IRSL and elevated temperature post-IR IRSL measurements (Spooner, 1994). The efficacy of such measures for excluding gypsum- or anhydrite-signal dominated aliquots, however, has not been tested.

2. Methodology

Samples were collected from two endorheic basins, Al Marrat and Jubbah, located near the southern edge of the An Nefud sand sea (Saudi Arabia) (Petraglia et al., 2011, 2012). Gypsum-rich samples (JB2-OSL2: 1.57 m, JB2-OSL5: 4.15 m) were collected from palaeoenvironmental sampling site JB-2 in the Jubbah basin, an 8.5 m section comprising carbonate-rich and gypsiferous sediments, sands, and clays. Field observations indicated extensive gypsum precipitation within the upper four to five meters of this section, with crystals up to several centimeters in size. During sampling, however, an effort was made to avoid the most gypsiferous units, and samples were collected from powdery carbonate units. It was presumed that these carbonate units might be more likely to include quartz and feldspar grains. Collection and initial preparation methods for nominal 'quartz' and 'feldspar' coarse grain fractions (180 – 255 µm) followed Hilbert et al. (2014), and included wet sieving, digestion in hydrochloric acid, a sodium polytungstate separation (ρ = 2.58 g cm^{-3}), and ninety minutes hydrofluoric acid etching for the quartz fraction.

Subsequently, these samples were prepared with a second sodium polytungstate separation (ρ = 2.35 g cm^{-3}) in order to further separate pure gypsum crystals. The efficacy of these density separations will be discussed later. In the results and discussion, mineral fractions will be referred to by density (e.g. $\rho < 2.58$ or $\rho < 2.35$ g cm^{-3}). Typical Nefud coarse-grained quartz (Q) and feldspar (F) separates (180 – 255 µm) were extracted from luminescence samples collected in sand-rich deposits in the nearby Al Marrat basin and Jubbah basin site Al-Rabyah (Hilbert et al., 2014), respectively. These were prepared according to the first method described above.

All equivalent dose (D_E) measurements were performed with either a lexsyg research or a lexsyg smart (Richter et al., 2013). Standard BSL SAR (Murray & Wintle, 2000, 2003), $pIRIR_{290}$ SAR (Thiel et al., 2011), and modified low temperature BSL and IRSL SAR protocols (similar to

Set	Stim./Detection	Use	Filters
1	BSL/UV_{340}	Standard BSL SAR	Hoya U340 glass (2.5 mm) + Delta-BP 365/50 EX-interference (5 mm)
2	$IRSL\&pIRIR_{290}$	Standard $IRSL_{50}$ and $pIRIR_{290}$	Schott BG 39 glass (3 mm) + AHF Brightline HC414/46-interference (3.5 mm)
3	BSL/UV_{330}	Gypsum characterization (RT)	Hoya U340 glass (2.5 mm) + AHF Brightline HC340/26 Interference (5 mm)
4	BSL/UV_{380}	Gypsum characterization (RT)	Hoya U340 glass (2.5 mm) + Delta-BP 365/50 EX-Interference (5 mm)
5	$IRSL/UV_{330}$	Gypsum characterization (50 °C)	Hoya U340 glass (2.5 mm) + AHF Brightline HC340/26 Interference (5 mm)
6	IRSL/blue	Gypsum characterization (50 °C)	Schott BG 39 glass (3 mm), Schott BG 25 (3 mm), Schott KG3, (2 mm)

Table 1. Filter combinations used for measurements.

O'Connor et al. 2011) were tested for various mineral fractions. Measurement parameters and luminescence signal integration limits are given in Tables 1 and 2, and data were analysed with Luminescence Analyst v. 4.11. Detection/emission combinations are referred to in the text as, e.g., BSL/UV_{330}: blue light stimulation with emission detection centered at 330 nm. Though the gypsum will be at least partially dehydrated by heating, we will refer to non-quartz and feldspar aliquots both pre- and post-heating as either gypsum or gypsum-rich.

3. Results and Discussion

Initial BSL and $pIRIR_{290}$ measurements upon mineral separates ($\rho < 2.58$ g cm^{-3} and $\rho < 2.58$ g cm^{-3}, respectively) from samples JB2-OSL1 and JB2-OSL2 yielded either negligible or anomalous signals (see discussion below and Figure 3). This prompted the mineralogical investigations and luminescence characterization reported here. As a first step, the purity of each fraction was investigated via scanning electron microscopy. Previously measured aliquots from both samples were carbon coated and examined for grain morphology and composition. Many crystals displayed morphology typical of gypsum (Mees et al., 2012), with elongated shapes (> 600 µm) or smaller, broken crystal forms (Figure 1). Spectral analysis confirmed the dominant presence of gypsum with some quartz or feldspar grains in both fractions. Nominal 'quartz' aliquots ($\rho > 2.58$ g cm^{-3}) comprised half or more gypsum grains, while nominal 'feldspar' aliquots ($\rho < 2.58$ g cm^{-3}) comprise primarily gypsum, with infrequent feldspar and quartz grains. Mahan & Kay (2012) also described poor results from density separation of gypsum-rich samples and attributed this to gypsum overgrowth upon denser minerals such as quartz. It seems possible, too, that the sheer amount of gypsum in these samples might have trapped denser grains during density separation, though samples were stirred gently to discourage grain clumping and then centrifuged for at least 5 minutes. It can also be noted that SEM images of the gypsum crystals do not show any pits indicative of hydrofluoric or hydrochloric acid etching. Gypsum reaction with hydrofluoric acid seems to be negligible at room temperature during the 90 minute etch used here; this is in contrast to HF etching of quartzes and feldspars which results from the conversion of silicates into fluorosilicates (Fogler et al., 1975). Indeed, chemical removal of gypsum precipitates requires extensive treatment with high strength acids, for instance, treatment by ethylene diamine tetra acetic acid followed by digestion in heated 12 N HCl for three hours (Kocurek et al., 2007; Mahan & Kay, 2012).

We then confirmed that these gypsum-rich aliquots ($\rho < 2.58$ g cm^{-3}, sample JB2-OSL5) yielded a luminescence signal if measured at room temperature (RT). Three aliquots (6 mm diameter) were bleached with both blue (100 s) and IR LEDs (300 s) at room temperature, after which each underwent several cycles of irradiation (27.8 Gy) and luminescence detection with various stimulation/emission parameters (Tables 1 and 2): BSL/UV_{330}, BSL/UV_{380}, IRSL/UV_{330}, and IRSL/blue. Luminescence decay curves are shown in Figure 2a. Absolute signal strength and relative magnitude of the tested signals were similar for all three aliquots. BSL/UV_{380} provided the strongest signal, with an initial magnitude of approximately 1000 counts per 0.1 s. BSL/UV_{330} was the next strongest, with a signal approximately 60 % of the BSL/ UV_{380} signal, followed by IRSL/blue (20 %). IRSL/UV_{330} provided by far the weak-

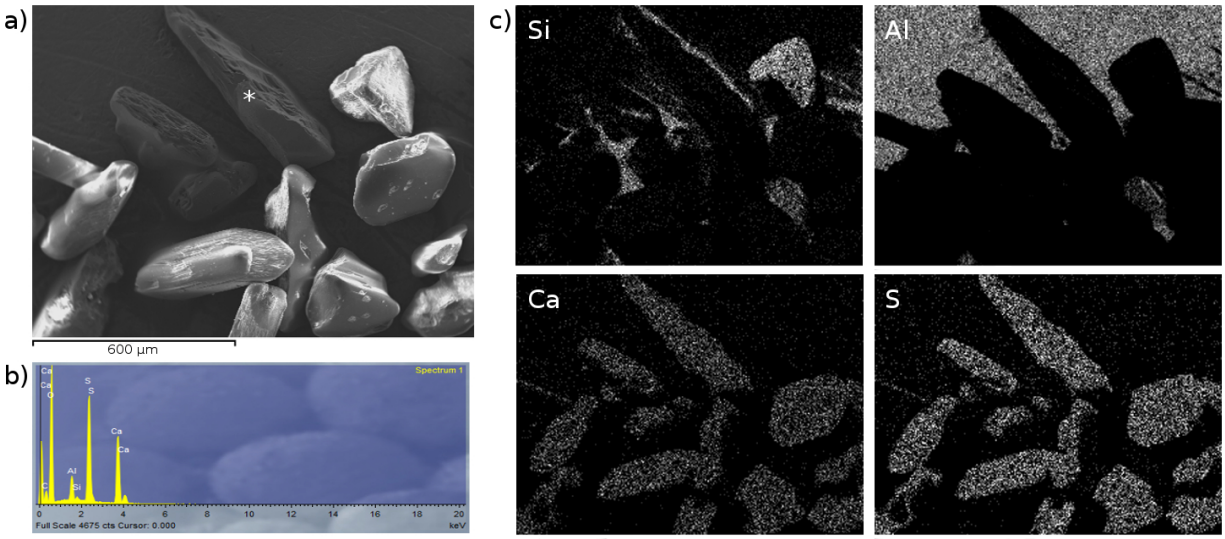

Figure 1. SEM image of JB2-OSL5 aliquot ($\rho < 2.58$ g cm^{-3}). Nearly all of the crystals in the view are gypsum, based on the elemental compositions shown in (c) and crystal morphology. The spectrum shown in b) was collected at the point marked with the white star in a). The crystal on the upper right is quartz, and no feldspars are visible. Silicon rims around many of the grains are due to the use of silicone oil in aliquot preparation.

SAR Step	Standard BSL	$pIRIR_{290}$	Modified BSL	Modified IRSL
1	β irradiation	β irradiation	β irradiation	β irradiation
2	Preheat 260 °C (5 °C s^{-1}, hold 10 s)	Preheat 320 °C (5 °C s^{-1}, hold 60 s)	Pause 10000 s	
3	IRSL (IR depletion step only) 50 °C, 100 s	IRSL[2] 50 °C, 200 s Signal: first 2 s Background: last 50 s	BSL[4] RT, 100 s stimulation Signal: first 1.5 s Background: last 30 s	IRSL[6] 50 °C, 300 s Signal: first 2.5 s Background: last 100 s
4	BSL[1] 125 °C, 60 s Signal: first 0.2 s Background: last 20 s	IRSL[2] 290 °C, 200 s Signal: first 2 s Background: last 50 s		
5	β irradiation	β irradiation	β irradiation	β irradiation
6	Preheat 240 °C (5 °C s^{-1}, hold 10 s)	Preheat 320 °C (5 °C s^{-1}, hold 60 s)	Pause 10000 s	
7	BSL[1] As above	IRSL[2] 50 °C as above	BSL[4] As above	IRSL[6] 50 °C as above
8	Hot Bleach 280 °C, 100 s blue LED stimulation	IRSL[2] 290 °C as above		
9		Hot Bleach 325 °C, 100 s IR LED stimulation		

Table 2. Stimulation and heating parameters for regeneration protocols. Aliquots were prepared in the following sizes (left to right): 2 mm, 1 mm, 6 mm, 6 mm.

est signal, with a relative strength of only 3 %. In all cases, a significant BSL signal could still be measured after IRSL stimulation.

Regeneration curves were then measured for both BSL/UV_{380} (RT) and IRSL/blue combinations (50 °C, Figure 2b), using a modified SAR protocol with no preheat (Table 2). For comparison, representative growth curves are shown for typical quartz (BSL SAR with preheat) and feldspar ($pIRIR_{290}$) aliquots as well. It is evident that both gypsum regeneration curves have a higher D_0 than Nefud quartz or feldspar samples, with the IRSL/blue curve yielding the highest saturation point. The highest dose given in the laboratory was 1113 Gy, at which point the normalized IRSL/blue signal was not yet saturated. The D_0 calculated for this aliquot was ca. 1500 Gy. Recycling ratios for both regeneration curves were within two sigma of unity (IRSL/blue: 1.16 ± 0.10; BSL/UV_{380}: 0.99 ± 0.05). Recuperation levels were also low, being negative for IRSL/blue detection and only 5.7 ± 0.9 % for BSL/UV_{380}.

It seems probable that these signals derive primarily from gypsum rather than quartz or feldspar inclusions. Based on SEM results, we know that rare quartz and feldspar grains are included in this fraction, however, no feldspar or quartz grains were identified when aliquots were inspected under a microscope. Of course, this cannot rule out the presence of microscopic mineral inclusions. Yet recorded luminescence characteristics correspond closely to those reported in the literature for natural and synthetic gypsum (Detschel & Lepper, 2009; O'Connor et al., 2011). Examination of TL measurements for several aliquots from this fraction did not show a measurable 110 °C peak (i.e. an indication of the presence of quartz grains). Finally, another aliquot of the purified gypsum fraction ($\rho < 2.35$ g cm^{-3}, sample JB2-OSL5) was prepared, irradiated (524.4 Gy), and its luminescence signal was measured with an EMCCD camera incorporated into a lexsyg research at the Stockholm Luminescence Laboratory (IRSL stimulation at 50 °C, 1.9 s exposure, blue filter set). No emission centers were detected in the resulting image, suggesting that no feldspar inclusions are present; by comparison another gypsum-rich sample with suspected feldspar inclusions was measured and multiple, bright IRSL responsive grains were detected. All evidence suggests that quartz and feldspar inclusions seem to be rare in JB2-OSL5 gypsum grains. Based on grain morphology, we suspect that the most of this sample's gypsum crystallised within a water column and limited the presence of mineral inclusions, however, more research is necessary to prove this.

We then tested the gypsum's luminescence response to typical elevated temperature BSL with preheating, as is often used for quartz luminescence dating. Two aliquots were prepared from the purified gypsum fraction ($\rho < 2.35$ g cm^{-3}, JB2-OSL5) and measured with a full SAR BSL protocol (Tables 1 and 2, Figure 3a). Additionally, twelve aliquots of the primarily gypsiferous 'heavy' fraction ($\rho > 2.58$ g cm^{-3} JB2-OSL2) were prepared and measured with variable stimulation power and integration time (50 or 100 mW cm^{-2}, 0.1 s or 0.5 s per channel). For this second group, only the natural signal and one regeneration dose (152.4 Gy) were measured, with a test dose of 30.5 Gy. All aliquots shared the same characteristics, therefore they are discussed together.

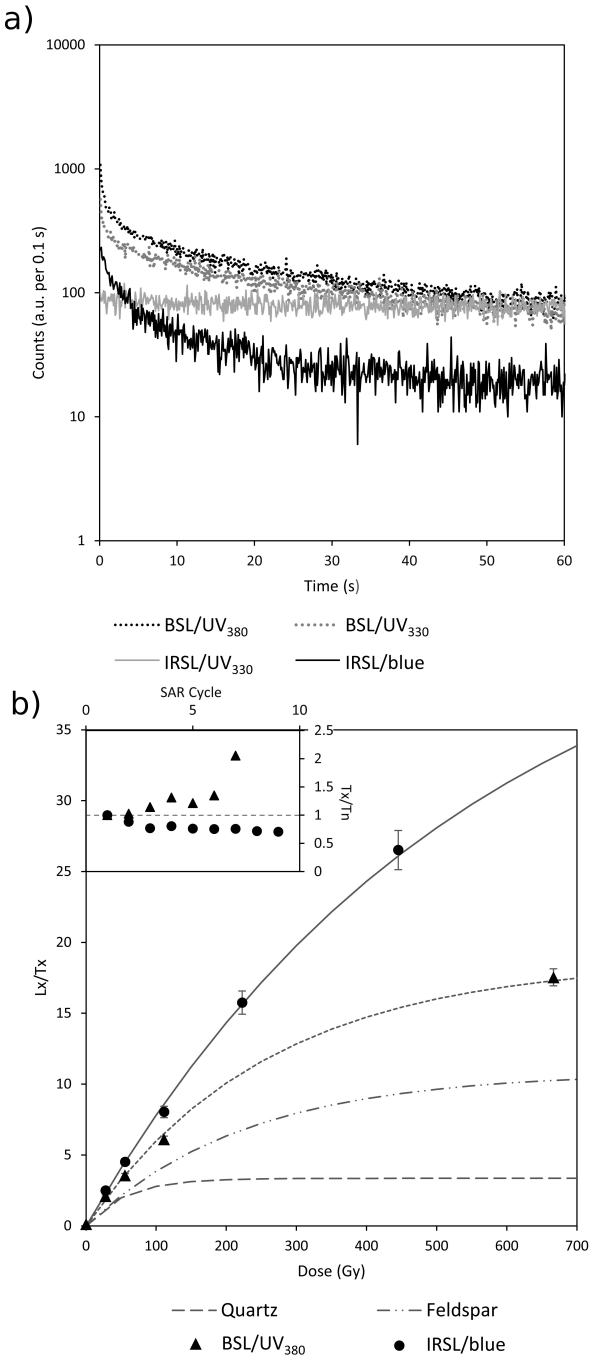

Figure 2. Gypsum luminescence signals. A) Luminescence decay curves recorded at room temperature with various stimulation/detection combinations. B) Regeneration curves and test dose sensitivity changes (inset) measured for gypsum at low temperature (BSL/UV_{380} at room temperature, IRSL/blue at 50 °C) compared to typical quartz BSL/UV_{340} and feldspar $pIRIR_{290}$ curves.

Natural signals of the gypsum-rich separates measured via the typical BSL/UV_{340} quartz SAR protocol were measurable but insignificant. A small initial signal is present (on the order of 150 counts per 0.1 s), but this is more than an order of magnitude less intense than the signal from a typical pure quartz aliquot (Figure 3a). Test doses of up to 29.8 Gy did not yield measurable signals (greater than 3 times the standard deviation above the background level), therefore such aliquots would typically be rejected according to standard rejection criteria. Regeneration doses did produce higher signal levels (e.g. 200 counts per 0.1 s after 299.9 Gy irradiation) however, no growth curve could be constructed due to the lack of test dose signal. By contrast, the reference quartz aliquot yields measurable test dose signals with increasing sensitivity, a regeneration curve well fit by a saturating exponential, good recycling ratio and zero ratios, with no evidence for feldspar contamination (IR depletion ratio). Based on these characteristics, it is unlikely that the low-strength gypsum signal will adversely affect D_E's measured from accepted quartz aliquots. In the case that mineral separation is very poor and only one or a very few quartz grains are included in an aliquot, we suggest that the test dose sensitivity change can be a useful additional rejection criterion. Evidence discussed below and results from Jain et al. (2006) and Mahan & Kay (2012) indicate that a gypsum-dominated signal will show a precipitous decrease in sensitivity after heating to such temperatures, whereas quartz usually increases sensitivity through the SAR cycle (Jungner & Bøtter-Jensen, 1994; Murray & Wintle, 2000).

Two more aliquots were prepared from the purified gypsum fraction ($\rho < 2.35$ g cm^{-3}, JB2-OSL5) and measured according to the $pIRIR_{290}$ protocol (Tables 1 and 2). Ten aliquots each from JB2-OSL2 and JB2-OSL5 ($\rho < 2.58$ g cm^{-3}) were also measured via $pIRIR_{290}$. As above, luminescence characteristics were similar for all three sets of aliquots, therefore they are discussed together.

No signal was detected during IRSL (50 °C) stimulation in either the natural or regenerated measurements; the signal is noisy and never greater than 50 counts per 0.4 s (Figure 3, inset). This value is less than the typical background level of a known feldspar aliquot after 200 s stimulation. When subjected to a subsequent IRSL stimulation at 290 °C, however, gypsum-rich aliquots yield a detectable signal of approximately 500-1000 counts per 0.4 s (Figure 3). The form of this decay is quite different from a typical $pIRIR_{290}$ feldspar signal, and seems to consist entirely of medium and slow components (though no deconvolution was performed). The $pIRIR_{290}$ signal of gypsum also differs from feldspar in that sensitivity dramatically decreases through the SAR cycle: after seven cycles the magnitude of the test dose signal may be ∼10 % or less of the first test dose. High thermal recuperation, between 20 % and 60 % of L_N/T_N ($\mu \pm \sigma$: 41.6 ± 9.8 %), is also a consistent feature.

4. Conclusions

It is important to note that gypsum-rich aliquots yield a detectable signal of approximately 500 – 1000 counts per 0.4 s when measured with IRSL stimulation at 290 °C. We suggest, however, that pure or nearly pure luminescence signals from quartz and feldspar minerals can be detected via the application of standard rejection criteria to BSL/UV_{340} and $pIRIR_{290}$ SAR data, respectively. Aliquots with a sig-

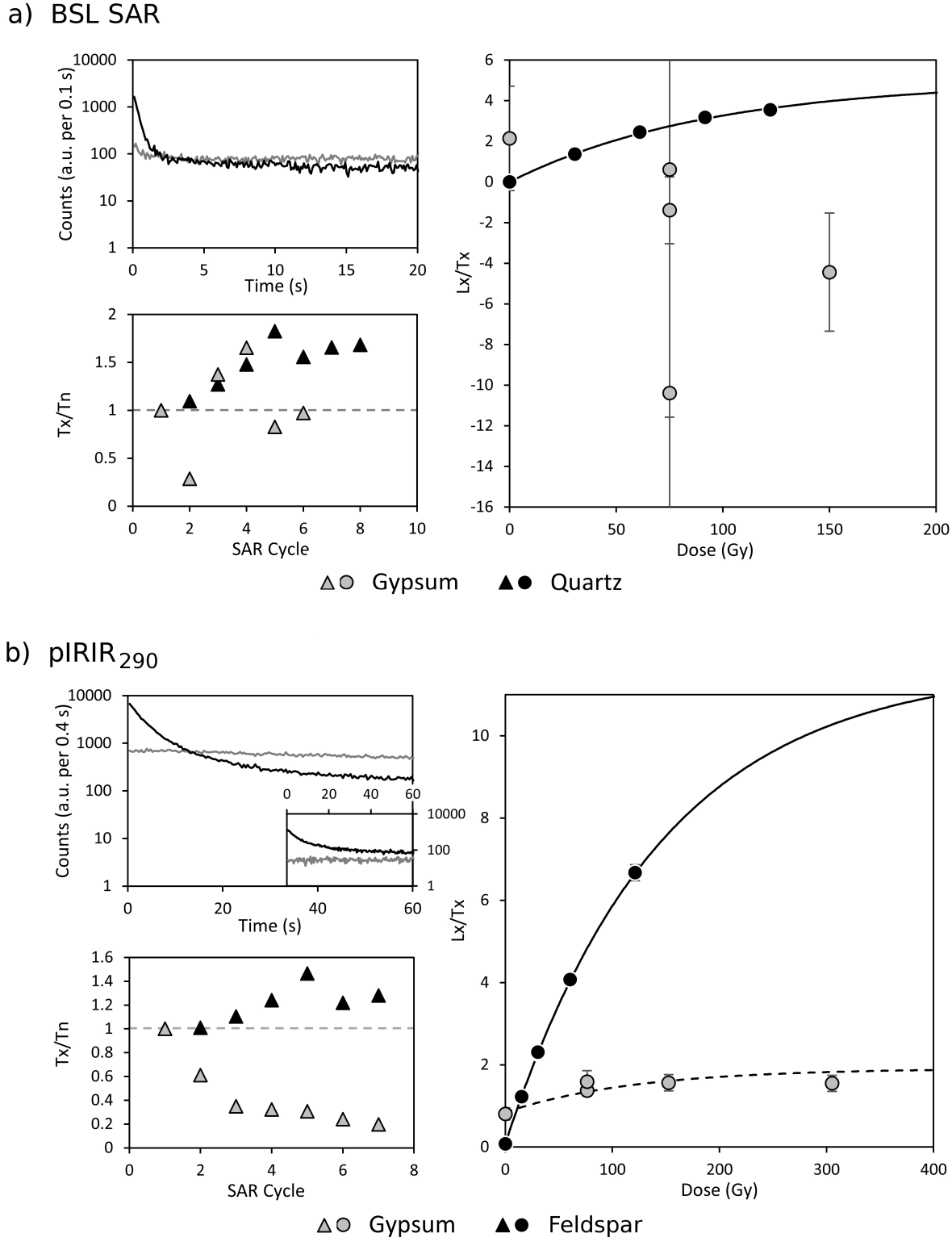

Figure 3. Gypsum-rich aliquots measured with standard BSL/UV_{340} SAR protocol (a) and $pIRIR_{290}$ protocol (b). Gypsum natural decay curves, test dose sensitivity changes, and regeneration curves are plotted in comparison to quartz (a) or feldspar (b). The inset box in (b) shows the natural IRSL (50 °C) signal. Note that several higher regenerated doses (gypsum) are not shown.

nal dominated by gypsum will fail several rejection criteria, particularly:

- detectable natural test signal greater than three sigma above the background signal (BSL)
- test dose error less than 15 – 20 % of the calculated test dose (BSL)
- calculated zero-ratio less than 5 % of L_N/T_N ($pIRIR_{290}$)

Inspection of the decay curve form and test dose sensitivity change should also be conducted if gypsum contamination is suspected, and aliquots with significant sensitivity decrease excluded from further consideration. It may still be prudent to be wary of dates calculated for either quartz or feldspar minerals extracted from a gypsiferous layer if gypsum overgrowth occurs. Grain size estimates are important for attenuation factors and the calculation of internal dose rates for K-feldspars. Gypsum overgrowth will also inhibit hydrofluoric acid etching of quartz, which may lead to dose rate inaccuracies. This issue must be evaluated for each site, however, and is outside the scope of this paper.

Acknowledgments

We thank HRH Prince Sultan bin Salman, President of the General Commission for Tourism and Antiquities, and Professor Ali I. Al-Ghabban, Vice President for Antiquities and Museums, for permission to carry out this study. We also thank Jamal Omar and Sultan Al-Fagir of the Saudi Commission for Tourism and National Heritage (SCTH), and the people of Jubbah for their support and assistance with the field investigations. We acknowledge financial support from the European Research Council (grant no. 295719, to Michael Petraglia) and from the SCTH. Finally, we thank Chris Doherty of the Research Laboratory for Archaeology and the History of Art (University of Oxford) for his assistance with the SEM and Professor Frank Preusser and Natacha Gribenski (University of Stockholm) for use of EMCCD imaging facilities.

References

Aydaş, C., Engin, B., and Aydin, T. *Radiation-induced signals of gypsum crystals analysed by ESR and TL techniques applied to dating*. Nuclear Instruments and Methods in Physics Research, Section B: Beam Interactions with Materials and Atoms, 269(4): 417–424, 2011. doi: 10.1016/j.nimb.2010.12.074.

Detschel, M. and Lepper, K. *Optically stimulated luminescence dating properties of Martian sediment analogue materials exposed to a simulated Martian solar spectral environment*. Journal of Luminescence, 129(4): 393–400, 2009. doi: 10.1016/j.jlumin.2008.11.008.

Duller, G. *Distinguishing quartz and feldspar in single grain luminescence measurements*. Radiation Measurements, 37(2): 161–165, 2003. doi: 10.1016/S1350-4487(02)00170-1.

Fogler, H., Lund, K., and McCune, C. *Acidization III-The kinetics of the dissolution of sodium and potassium feldspar in HF/HCl acid mixtures*. Chemical Engineering Science, 30: 1325–1332, 1975. doi: 10.1016/0009-2509(75)85061-5.

Hilbert, Y., White, T., Parton, A., Clark-Balzan, L., Crassard, R., Groucutt, H., Jennings, R., Breeze, P., Parker, A., Shipton, C., Al-Omari, A., Alsharekh, A., and Petraglia, M. *Epipalaeolithic occupation and palaeoenvironments of the southern Nefud desert, Saudi Arabia, during the Terminal Pleistocene and Early Holocene*. Journal of Archaeological Science, 50(1): 460–474, 2014. doi: 10.1016/j.jas.2014.07.023.

Jain, M., Andersen, C., Bøtter-Jensen, L., Murray, A., Haack, H., and Bridges, J. *Luminescence dating on Mars: OSL characteristics of Martian analogue materials and GCR dosimetry*. Radiation Measurements, 41(7-8): 755–761, 2006. doi: 10.1016/j.radmeas.2006.05.018.

Jungner, H. and Bøtter-Jensen, L. *Study of sensitivity change of OSL signals from quartz and feldspars as a function of preheat temperature*. Radiation Measurements, 23(2-3): 621–624, 1994. doi: 10.1016/1350-4487(94)90110-4.

Kocurek, G., Carr, M., Ewing, R., Havholm, K., Nagar, Y., and Singhvi, A. *White Sands Dune Field, New Mexico: Age, dune dynamics and recent accumulations*. Sedimentary Geology, 197 (3-4): 313–331, 2007. doi: 10.1016/j.sedgeo.2006.10.006.

Lager, G. A., Armbruster, T., Rotella, F. J., Jorgensen, J. D., and Hinks, D. G. *A crystallographic study of the low-temperature dehydration products of gypsum, $CaSO_4 \cdot 2H_2O$: hemihydrate $CaSO_4 \cdot 0.5H_2O$, and $\gamma - CaSO_4$*. The American Mineralogist, 69: 910–918, 1984.

Mahan, S. and Kay, J. *Building on previous OSL dating techniques for gypsum: A case study from Salt Basin playa, New Mexico and Texas*. Quaternary Geochronology, 10: 345–352, 2012. doi: 10.1016/j.quageo.2012.02.001.

Mathew, G., Gundu Rao, T., Sohoni, P., and Karanth, R. *ESR dating of interfault gypsum from Katrol hill range, Kachchh, Gujarat: Implications for neotectonism*. Current Science, 87(9): 1269–1274, 2004.

McLeod, L., Rudowski, R., and Ullman, W. *Pure gypsum separates from 'dirty' evaporites*. Research Methods Papers, pp. 596–597, 1985.

Mees, F., Casteñeda, C., Herrero, J., and Van Ranst, E. *The nature and significance of variations in gypsum crystal morphology in dry lake basins*. Journal of Sedimentary Research, 82(1): 37–52, 2012. doi: 10.2110/jsr.2012.3.

Murray, A. and Wintle, A. *Luminescence dating of quartz using an improved single-aliquot regenerative-dose protocol*. Radiation Measurements, 32(1): 57–73, 2000. doi: 10.1016/S1350-4487(99)00253-X.

Murray, A. and Wintle, A. *The single aliquot regenerative dose protocol: Potential for improvements in reliability*. Radiation Measurements, 37(4-5): 377–381, 2003. doi: 10.1016/S1350-4487(03)00053-2.

Nagar, Y., Sastry, M., Bhushan, B., Kumar, A., Mishra, K., Shastri, A., Deo, M., Kocurek, G., Magee, J., Wadhawan, S., Juyal, N., Pandian, M., Shukla, A., and Singhvi, A. *Chronometry and formation pathways of gypsum using Electron Spin Resonance and Fourier Transform Infrared Spectroscopy*. Quaternary Geochronology, 5(6): 691–704, 2010. doi: 10.1016/j.quageo.2010.05.001.

Nambi, K. *ESR and TL dating studies on some marine gypsum crystals*. PACT, 6: 314–321, 1982.

O'Connor, V., Lepper, K., Morken, T., Thorstad, D., Podoll, A., and Giles, M. *A survey of the signal stability and radiation dose response of sulfates in the context of adapting optical dating for Mars*. Journal of Luminescence, 131(12): 2762–2768, 2011. doi: 10.1016/j.jlumin.2011.06.031.

Petraglia, M., Alsharekh, A., Crassard, R., Drake, N., Groucutt, H., Parker, A., and Roberts, R. *Middle Paleolithic occupation on a Marine Isotope Stage 5 lakeshore in the Nefud Desert, Saudi Arabia*. Quaternary Science Reviews, 30: 1555–1559, 2011.

Petraglia, M., Alsharekh, A., Breeze, P., Clarkson, C., Crassard, R., Drake, N., Groucutt, H., Jennings, R., Parker, A., Parton, A., Roberts, R., Shipton, C., Matheson, C., Al-Omari, A., and Veall, M.-A. *Hominin dispersal into the Nefud Desert and Middle Palaeolithic Settlement along the Jubbah Palaeolake, Northern Arabia*. PLoS ONE, 7(11): e49840, 2012.

Richter, D., Richter, A., and Dornich, K. *Lexsyg A new system for luminescence research*. Geochronometria, 40(4): 220–228, 2013. doi: 10.2478/s13386-013-0110-0.

Spooner, N. *On the optical dating signal from quartz*. Radiation Measurements, 23(2-3): 593–600, 1994. doi: 10.1016/1350-4487(94)90105-8.

Thiel, C., Buylaert, J., Murray, A., Terhorst, B., Hofer, I., Tsukamoto, S., and Frechen, M. *Luminescence dating of the Stratzing loess profile (Austria) - Testing the potential of an elevated temperature post-IR IRSL protocol*. Quaternary International, 234(1-2): 23–31, 2011. doi: 10.1016/j.quaint.2010.05.018.

Warren, J. *Evaporites: Sediments, resources, and hydrocarbons*. Springer, Berlin, 2006. ISBN 9783540260110.

Reviewer

Shannon Mahan

Ancient TL

Sources of variability in single grain dose recovery experiments: Insights from Moroccan and Australian samples

Nina Doerschner[1]*, Marion Hernandez[1], Kathryn E. Fitzsimmons[1]

[1] Department of Human Evolution, Max Planck Institute for Evolutionary Anthropology
Deutscher Platz 6, D-04103 Leipzig, Germany

*Corresponding Author: nina_doerschner@eva.mpg.de

Received: April 12, 2016; in final form: June 10, 2016

Abstract

In our study, we investigate the quartz single-grain dose recovery characteristics of five aeolian samples from three archaeological sites in Australia and Morocco. Comparatively small (20 – 49 Gy) and high (180 – 208 Gy) doses were applied to sand-sized quartz grains of each sample. Samples were bleached by green laser, sunlight and solar simulator stimulation. We observed a primary dependency of the results on the size of the administered dose, but also observed sample-specific responses to the chosen dose recovery measurement parameters.

The Australian samples originate from an open-air archaeological site and consist of highly sensitized quartz grains with comparatively small equivalent doses. By contrast, the Moroccan samples originate from two cave sites known to be affected by heterogeneous dose rates and post-depositional mixing to varying degrees; this material is generally less sensitive, and expected equivalent doses are >180 Gy, while single-grain quartz weighted average signal saturation levels ($2D_0$) exceed 235 Gy.

Single grains from all sites, with one exception, recover small applied laboratory doses. These fall within 5 % of unity irrespective of the bleaching method. However, when applied doses are high, dose recovery test results vary substantially depending on how individual samples respond to the bleaching treatment prior to the given dose. The lowest dose recovery ratios and highest overdispersion values were observed in samples bleached in the solar simulator. Our results highlight the importance of investigating dose recovery characteristics at single grain level, and indicate additional sources of complexity in understanding the luminescence characteristics of quartz.

Keywords: OSL, single grain, quartz, SAR, dose recovery test, artificial bleaching, overdispersion

1. Introduction

In recent years, dating of single sand-sized grains of quartz using optically stimulated luminescence (OSL) has been frequently applied in geological and archaeological contexts. By reducing the aliquot size for equivalent dose (D_e) determination from multigrain aliquots to individual grain level, better resolution of dose distributions can be obtained.

The overdispersion value (σ_{OD}) allows quantification of the variability observed in single grain dose distributions (Galbraith et al., 1999), comprising both extrinsic (dose rate heterogeneity, incomplete bleaching and post depositional mixing) and intrinsic factors, such as counting statistics, instrument reproducibility, thermal transfer or other sample-specific OSL characteristics (Thomsen et al., 2007). Especially when dating material from highly complex settings such as cave sites, σ_{OD} of an individual sample can yield significant insight into, for example, the depositional history of sediments, thereby improving the reliability of age determinations (Jacobs et al., 2012).

Dose recovery experiments are one of the standard performance tests in quartz OSL dating, and are commonly assumed to represent a useful check of the suitability of mea-

surement protocol parameters and the reliability of natural D_e estimates (Murray & Wintle, 2003).

In dose recovery experiments, known laboratory doses, which are recommended to be close to the expected natural D_e of a certain sample (Murray & Wintle, 2003), are administered either to artificially bleached or modern analogous samples. Their ability to recover this given dose within acceptable ranges – calculated as a ratio normalized to the applied dose – is assessed. Thomsen et al. (2012) have shown that the size of the administered dose is of considerable importance in dose recovery tests for single grains as well as for multiple grain aliquots. They found that, their quartz samples recovered relatively small given doses within unity, but at higher administered doses of 103 and 208 Gy, dose recovery was substantially underestimated by 10 – 15 %. As dose recovery tests are by definition laboratory-based experiments, the observed σ_{OD} in resulting single grain dose distributions only reflects the intrinsic variability in the individual sample and is not influenced by extrinsic factors, as is the case for natural samples (Thomsen et al., 2007). Furthermore, Guérin et al. (2015) recently found no correlation between dose recovery ratios and accuracy for obtained ages in 19 single-grain samples with independent age control. These observations cast doubt on the standard dose recovery test as a check for sample reliability, and highlight a need to investigate dose recovery tests in greater depth.

Given the complex nature of many cave-based archaeological sediments, dose recovery tests are often undertaken by resetting the natural signal rather than using modern analogues. Resetting can be achieved by various light sources which simulate natural bleaching conditions. The most commonly used bleaching sources are natural sunlight, solar simulators (SOL2), and stimulation in the OSL reader by green lasers or blue light emitting diodes (LEDs) (e.g. Aitken & Smith, 1988; Ballarini et al., 2007; Kang et al., 2012; Li & Wintle, 1991, 1992). Solar simulators (SOL2) have recently been shown to cause inaccuracies in dose recovery tests on multigrain aliquots (Choi et al., 2009; Wang et al., 2011). Thomsen et al. (2016) on the other hand, observed no significant systematic differences in dose recovery test results after SOL2 and blue LED bleaching for both, single grains and multigrain aliquots.

As yet it is unclear whether experimental dose recovery tests using artificial bleaching sources can accurately recover dose for all samples, especially in single grains, since generally dose recovery tests are undertaken on multigrain aliquots – even in a number of single grain dating studies (e.g. Arnold & Demuro, 2015; Demuro et al., 2012; Jacobs et al., 2008).

In this study we undertook single grain dose recovery tests (e.g. natural D_es, signal intensities) on five sand-sized quartz samples from three different environmental settings from archaeological sites in Australia and Morocco. We investigate the dose recovery characteristics of these samples following different bleaching methods and after administering doses of different magnitude. We discuss the potential impact of experimental design and sample luminescence properties on the obtained results.

2. Instrumentation and sample characteristics

2.1. Instrumentation

All OSL measurements were undertaken using an automated Risø TL-DA-20 reader with a single grain attachment (Bøtter-Jensen et al., 2003), equipped with a calibrated $^{90}Sr/^{90}Y$ beta irradiation source (Bøtter-Jensen et al., 2000), and fitted with a 7.5 nm Hoya U-340 filter (Bøtter-Jensen, 1997). Individual grains were mounted on single grain sample discs containing 100 holes (300 µm diameter) on a 10 x 10 grid. Optical stimulation was provided by 10 mW 532 nm solid-state green laser beams for 1 s at 125 °C (90 % power, ∼50 W/cm^2 power density (Duller et al., 1999) and infrared LEDs (875 nm wavelength, ∼130 mW/cm^2 power density).

2.2. Samples

We investigated five samples from archaeological sites that were deposited by eolian processes. We used quartz of the 180 – 212 µm sand-size fraction. Samples were extracted by a combination of wet and dry sieving, followed by chemical treatment (HCl, H_2O_2, density separation and HF) under subdued red light.

Three samples originate from two archaeological cave sites in Morocco. L-EVA-1083 was collected at the inland site of Rhafas (Doerschner et al., in revision; Mercier et al., 2007; Wengler, 1993), and L-EVA-1218 and L-EVA-1221 from Thomas Quarry I (TQ I), located in aeolianite in Casablanca city on the Atlantic coast (Rhodes et al., 2006). Both sites are caves filled with Pleistocene sediments that were affected by post-depositional carbonate cementation and dose rate heterogeneity of varying degrees. The proportions of individual grains emitting detectable luminescence signals for natural D_e determination are 23 – 66 % for Rhafas and 6.8 – 31 % for TQ I samples (proportions reflect full suite of samples collected at Rhafas and TQ I). Furthermore, these samples yield particularly high D_0 values which allow reliable determination of natural D_e between 126 and 216 Gy (using the Central Age Model (CAM) proposed by Galbraith et al., 1999), with σ_{OD} reaching up to 47 % (Table 1).

We compare these samples with two dune samples from the open-air archaeological site at Lake Mungo (LM), Australia (L-EVA-1010 and -1012; Fitzsimmons et al., 2014). These two samples yield CAM-derived natural D_e values of 42 and 21 Gy respectively, and σ_{OD} of less than 25 % (Table 1). Although previous work has already demonstrated that these samples exhibit bright, rapidly decaying OSL signals typical of highly sensitive quartz and are therefore well suited to OSL dating (Fitzsimmons, 2011; Fitzsimmons et al., 2014), it has also been reported that variations in microdosimetry in sediments from this region might induce relatively high σ_{OD} values in natural D_e distributions (Lomax et al., 2007).

To examine the different sensitivity characteristics of the individual samples, the sensitivity of the first test dose response T_N (in counts/seconds/Gy) of each single grain, obtained after measurement of the natural signal, was plotted

Table 1. Results of natural D_e determination and dose recovery tests.

Sample	Natural equivalent dose				Given dose (Gy)	Test dose (Gy)	Dose recovery green laser				Dose recovery sunbleached				Dose recovery SOL2			
	n^1 (%)	D_e[2] (Gy)	σ_{OD}[2] (%)	D_0[3] (Gy)			n^1 (%)	recovery ratio[2]	σ_{OD}[2] (%)	D_0[3] ((Gy)	n^1 (%)	recovery ratio[2]	σ_{OD}[2] (%)	D_0[3] ((Gy)	n^1 (%)	recovery ratio[2]	σ_{OD}[2] (%)	D_0[3] ((Gy)
Lake Mungo																		
L-EVA-1010	16.7	42±1	24±2	65±3	49	10	24.0	0.95±0.01	7±1	67±3	18.2	0.96±0.01	6±1	65±4	18.7	0.95±0.01	10±1	63±6
					185	36	16.7	0.80±0.02	18±2	115±5	14.0	0.79±0.01	12±1	116±7	12.2	0.81±0.02	14±2	118±5
L-EVA-1012	9.0	21±1	24±3	73±9	20	4	21.5	0.96±0.01	6±1	72±3	18.5	0.97±0.01	9±1	53±3	10.1	0.94±0.01	11±1	63±7
					185	36	17.8	0.67±0.02	25±2	104±4	9.8	0.86±0.02	12±2	131±8	12.7	0.68±0.03	35±3	111±5
Rhafas																		
L-EVA-1083	4.1	216±12	36±4	208±16	20	4	11.2	0.97±0.01	9±1	51±5	6.3	0.83±0.02	22±2	76±11	6.5	0.99±0.02	10±2	59±7
					208	42	7.0	0.94±0.02	9±2	167±13	5.0	0.87±0.02	6±2	161±8	7.2	0.75±0.03	25±3	148±6
Thomas Quarry I																		
L-EVA-1218	3.9	126±9	47±5	118±7	20	4	16.7	0.93±0.01	5±1	47±3	4.1	0.91±0.02	8±2	40±3	7.5	1.04±0.02	7±2	75±5
					180	36	4.3	0.89±0.03	19±3	132±7	5.5	0.85±0.02	7±3	130±6	6.4	0.75±0.03	27±3	116±8
L-EVA-1221	4.4	153±7	34±4	149±6	20	4	16.8	0.95±0.01	6±1	49±3	4.3	0.93±0.02	9±2	59±6	11.2	0.97±0.01	9±1	59±5
					205	42	7.0	0.81±0.02	15±3	132±5	7.1	0.78±0.02	15±2	138±6	7.3	0.76±0.02	19±2	148±9

[1]Percentage of accepted grains.
[2]Determined using the Central Age Model (Galbraith et al., 1999).
[3]Weighted average D_0 value of the accepted D_es and standard error of the mean.

Table 2. Single grain characteristics of dose recovery experiments.

Sample	Given dose (Gy)	n^1	detectable signal[2] (100 %)	accepted grains (%)	No L_N/T_N intersection (%)	Remaining grains (100 %)	Dim grains[3] (%)	Recuperation > 5 % (%)	Recycling ratio (> 20 %) (%)	Depletion by IR (%)	D_e error > 30 % (%)	Grubbs test[4] (%)	$D_e > 2D0$ (%)
Lake Mungo													
L-EVA-1010	49	1800	1483 (82 %)	24.6	3.1	1072	17.0	0.8	57.8	19.5	4.3	0.1	0.6
	185	1800	1494 (83 %)	17.1	18.4	963	13.6	2.8	33.2	17.6	22.8	0.3	9.7
L-EVA-1012	20	2100	1504 (72 %)	22.2	0.2	1170	24.2	0.9	54.4	19.9	0.6	0.1	0.0
	185	2000	1525 (76 %)	17.5	18.9	972	18.6	4.4	31.0	19.7	18.3	0.1	7.8
Rhafas													
L-EVA-1083	20	2900	1447 (50 %)	14.7	0.3	1230	34.3	2.0	47.0	14.4	2.1	0.2	0.0
	208	2500	1343 (54 %)	11.9	14.2	990	22.3	22.1	34.1	9.6	7.5	0.2	4.1
Thomas Quarry I													
L-EVA-1218	20	2500	1451 (58 %)	14.1	0.3	1242	44.1	0.0	42.0	11.8	1.6	0.5	0.0
	180	2800	1884 (67 %)	7.9	25.8	1241	27.4	1.0	45.1	8.8	14.3	0.0	3.3
L-EVA-1221	20	2400	1530 (64 %)	14.8	0.4	1303	38.2	0.2	47.7	12.0	1.5	0.4	0.0
	205	3000	2309 (77 %)	9.3	23.3	1492	24.2	1.4	46.2	10.5	13.2	0.1	4.2

[1]Total number of grains measured per sample.
[2]Percentage of grains yielding an initial luminescence signal above background, and for which interpolation of the sensitivity-corrected natural signal using a single saturating exponential dose response curve resulted in finite dose estimates.
[3]Percentage of grains rejected due to insufficient test-dose signal.
[4]Percentage of grains identified as statistical outliers (Grubbs, 1950).

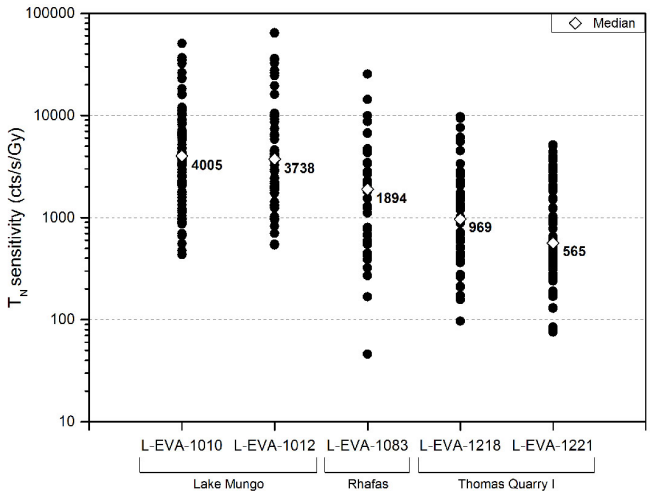

Figure 1. Luminescence sensitivity of single grains calculated from the OSL signal arising from the test dose immediately following natural D_e measurement (T_N) for all samples in this study (note logarithmic scale). Median values are indicated as open diamonds. Individual background corrected T_N signals were multiplied by 28.75 (1/0.035, integration in seconds) and then divided by the given test dose (Table S1) for comparability between samples.

(Fig. 1). Only individual grains accepted for natural D_e determination were incorporated to this figure; the test doses as applied to the samples using the single-aliquot regenerative-dose (SAR) protocol are listed in Table S1. The Australian samples yield high proportions of very bright grains ($> 10^4$ cts/s/Gy) and few grains emitting signal intensities of less than 10^3 cts/s/Gy. The samples from TQ I consistently yield single grain signal intensities in the range of $10^2 - 10^4$ cts/s/Gy. The sample L-EVA-1083 from Rhafas exhibits the most variable grain sensitivity; its calculated median sensitivity value is half that observed for the Australian samples.

In order to visualize the dominant OSL signal components in the samples, we undertook linearly-modulated OSL (LM-OSL) measurements on small (1 mm) aliquots at 125 °C using LEDs (470 nm, ∼40 mW/cm^2), following the procedure described by Bulur (1996). After preheating at 260 °C for 10 s, light intensity was increased from 0 to 90 % power over 500 s. The LM-OSL curves illustrate that all samples are dominated by the fast OSL signal component (Fig. S1). Single grain decay and growth curves of sample L-EVA-1221 (TQ I) and L-EVA-1010 (LM) also show that the samples are characterised by individual quartz grains with bright luminescence signals (Fig. 2). Weighted average D_0 values are higher in the Moroccan than the Australian samples. The determined D_e values – obtained using single saturating exponential curve fitting of the single grain dose response curves – for all samples in this study lie well below signal saturation levels (Table 1).

3. Dose recovery test – experimental details

Dose recovery tests on single grains were performed using the standard SAR protocol (Murray & Wintle, 2000, 2003) with a preheat temperature of 260 °C for 10 s, and a cutheat temperature of 220 °C. Preheat temperatures were determined based on the results of standard preheat plateau tests as well as combined dose recovery preheat plateau tests, in which seven different preheats (160 – 280 °C, data not shown) were applied to 1 mm multigrain aliquots (Murray & Wintle, 2003; Wintle & Murray, 2006). Potential feldspar contamination was tested at the end of each protocol by measuring the IR depletion of the OSL signal (Duller, 2003).

OSL signals were summed over the first 0.035 s of stimulation and corrected for background using the subsequent 0.035 s (Ballarini et al., 2007; Cunningham & Wallinga, 2009). Laboratory dose response curves were fitted using a single saturating exponential passing through the origin. Single grains were accepted for final analyses only when interpolation of the sensitivity-corrected natural signal on the dose response curve: 1) resulted in a finite dose estimate; 2) uncertainty on the natural test dose response was less than 20 % (test doses are given in Table 1); 3) were not affected by equivalent dose error > 30 %; and 4) passed the recuperation- (< 5 %), recycling- (< 20 %) and IR-depletion ratio tests (< 5 %). In addition, grains were rejected when exhibiting D_e signals exceeded saturation level (2 D_0) as suggested by Wintle & Murray (2006). Average dose recovery test ratios were calculated using the CAM.

Dose recovery tests were undertaken for each sample by applying two different laboratory doses and three different types of light exposure for bleaching. One applied dose was chosen to be close to the natural D_e (Murray & Wintle, 2003) and varied – depending on the sample – between 20 and 208 Gy (Table 1). A second set of dose recovery tests were performed for comparison using a laboratory dose of 185 Gy for the Australian samples (L-EVA-1010 and -1012) and 20 Gy for the Moroccan samples (L-EVA-1083, -1218 and -1221). Single grains from each sample were bleached by 1) the green laser (1 s at room temperature) in the OSL reader, 2) sunlight on the window sill (> 7 days, behind glass and therefore not entirely analogous to natural bleaching conditions), and 3) SOL2 at a lamp/sample distance of 60 cm. Stimulation in the Hönle solar simulator (equipped with a Hönle H2 filter, transmission range > 295 nm) by SOL2 was performed for 5 min to make sure that the individual grains were completely bleached while also avoiding underestimation of the recovered dose, as has been demonstrated for exposure times exceeding 1 hour (Choi et al., 2009). The total amount of individual grains measured for each dose recovery experiment is listed in Table S1.

4. Results

4.1. Acceptance and rejection of individual grains

Detailed information about the rejection of single grains for the different dose recovery experiments is listed in Ta-

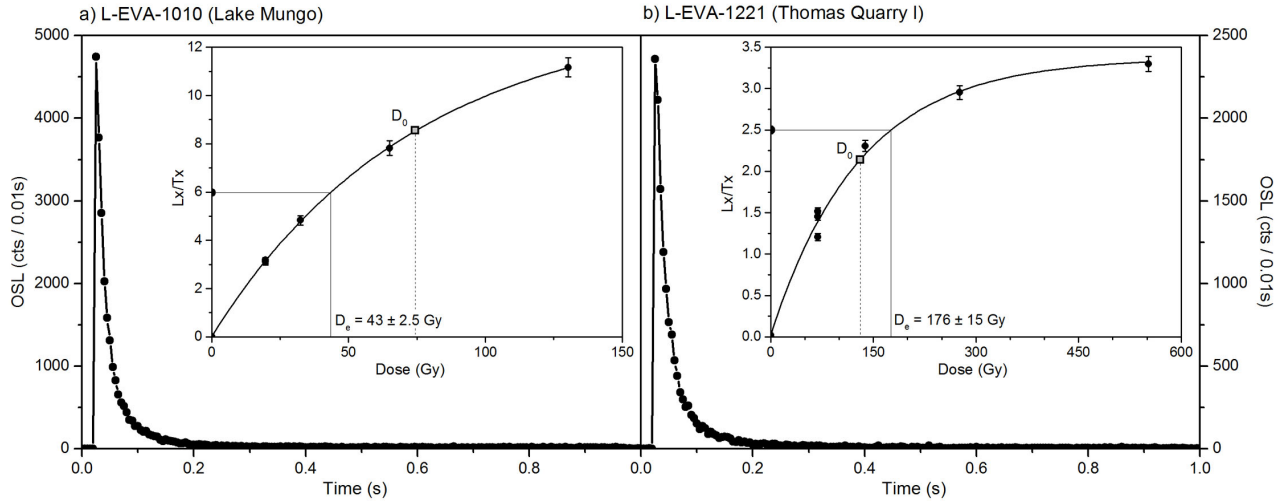

Figure 2. Natural OSL single grain decay and (as inset) dose-response curves for samples (a) L-EVA-1010 and (b) L-EVA-1221.

ble 2. Australian samples are more likely to give detectable luminescence signals for the chosen test doses (Table 1) than the Moroccan samples (LM 72 – 83 %, Rhafas 50 – 54 %, TQ I: 58 – 77 %, Table 2). This arises from the variability in intrinsic luminescence properties; the Australian samples generally comprise higher proportions of bright grains than the Moroccan samples (Fig. 1). Out of the grains exhibiting detectable luminescence signals, 14 to 26 % were rejected due to oversaturation (grains showing a L_n/T_n ratio well above maximum L_x/T_x value of the generated dose response curve) when administered doses are high (180 – 208 Gy), while this is only the case for 0.3 – 3.1 % of grains when administered doses are small (20 – 49 Gy). Sample L-EVA-1083 (Rhafas) yields the lowest rejection rate due to oversaturation at high given doses. This is most likely a consequence of its high signal saturation level after administration of a high dose, revealing weighted average D_0 values > 148 Gy in our dose recovery experiments (Table 1).

D_0 values calculated for all samples are consistent between bleaching types (Table 1). They do, however, show large variability depending on the given dose, with D_0 values arising from low administered doses yielding significantly smaller values than those arising from high doses. This is most likely caused by the different regeneration doses of the dose recovery measurements (Table S2). Maximum regeneration doses are considerably smaller after low given doses in comparison with high given doses. These results indicate that D_0 can presumably only be accurately determined when dose response curves are taken up to large doses.

Oversaturated grains were excluded from further analyses of rejection criteria in Table 2 to avoid statistical bias between dose recovery experiments with high and low given doses. As previously mentioned, regeneration doses vary in dose recovery experiments depending on the size of the given dose (Table S2). Therefore, observed differences in criteria causing rejection of individual grains between low and high given doses might partly be caused by those different measurement parameters. Depending on the sample site, individual grains are more likely to be rejected after a low administered dose due to poor recycling ratios (LM), insufficient test dose signals (TQ I) or a combination of both (Rhafas). While TQ I samples at high given doses only show a significant increase in rejection rates due to D_e errors exceeding 30 %, samples from LM are additionally affected by single grains failing the $2D_0$ criterion. Single grains from Rhafas increasingly fail due to recuperation values of > 5 %.

The number of individual grains passing all rejection criteria for dose determination varies considerably between sampling locations (LM: 10 – 24 %, Rhafas: 5 – 11 % and TQ I: 4 – 17 %; Table 1, Fig. 3a). Although a large number of single grains were rejected due to oversaturation solely when given doses were high, there is no clear correlation – with the exception of sample L-EVA-1010 (LM) – between the proportion of accepted grains and the size of the given dose. It is interesting to note that exceptionally high acceptance rates (11 – 24 %) were achieved for all samples when low doses were applied following green laser bleaching (Fig. 3a).

4.2. Differences observed in dose recovery ratios

Figure 3b summarizes the results of the measured/given ratios for each sample in the dose recovery experiment. The Australian samples from LM (L-EVA-1010 and -1012) and sample L-EVA-1221 from TQ I (Morocco) yield dose recovery ratios within 7 % of unity after low given doses, regardless of bleaching type (Fig. 3b, Table 1). By contrast, when given doses are high, these samples underestimate the measured/given ratios by 14 – 33 %. For the remaining Moroccan samples from Rhafas (L-EVA-1083) and TQ I (L-EVA-1218), recovery ratios vary between 1 – 17 % and 6 – 25 % of unity following low and high applied doses, respectively.

The type of bleaching source appears to influence dose recovery ratios for the Moroccan samples (Rhafas and TQ I). SOL2 stimulation at small given doses consistently results in values with the lowest (1 – 4 %) deviation from unity. Bleaching by sunlight results in the highest (7 – 17 %) devi-

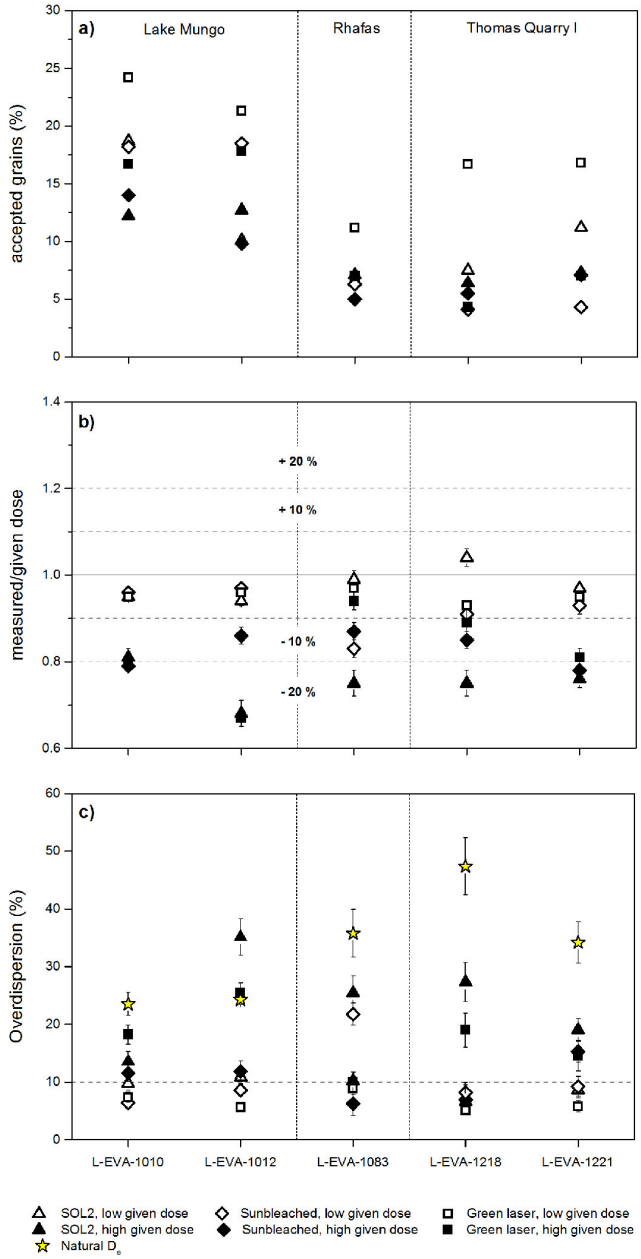

Figure 3. Results of single grain dose recovery experiments: (a) number of accepted grains after applying rejection criteria, (b) measured/given dose ratios and (c) calculated σ_{OD} values. Individual grains from each sample were bleached with green laser (squares), natural sunlight (diamonds) and SOL2 (triangles) prior to administering low (open symbols) or high (filled symbols) doses. Overdispersion values determined for the natural D_es are indicated by yellow stars.

ation of dose recovery from unity. Conversely, when given doses are high, green laser bleaching results in the most accurate (6 – 19 %) and SOL2 the least accurate (25 – 26 %) measured/given ratios. The Australian sample L-EVA-1012 (LM), however, yields consistent values of underestimation after high given doses for both, SOL2 and green laser bleaching (32 – 33 %).

To examine potential correlation between the degree of grain sensitivity and the accuracy of the dose recovery test results, measured/given ratios were plotted as a function of the corresponding single grain L_N signal intensities (Fig. S2). Individual grains from all samples emitting high intensity signals yield measured/given ratios close to unity when given doses are small. This characteristic decreases with decreasing signal intensity (Fig. S2a-e). The shape of the dose distributions, however, varies between samples. Individual grains from Rhafas (L-EVA-1083, Fig. S2c) are more widely scattered than LM or TQ I samples, whose distributions are relatively narrow. These results indicate a stronger correlation between signal intensity and accuracy of the dose recovery ratio. Similar single grain distributions following dose recovery experiments have also been observed in other studies (Duller et al., 2000; Jacobs et al., 2006; Thomsen et al., 2007). By contrast, when given doses are high, samples from all three sites exhibit a different behaviour. Single grains inconsistently over- and under-estimate the measured/given ratios, independently of L_N signal intensity (Fig. S2f-j).

The insets of Figure S2 show a correlation between measurement precision and L_N signal intensities for all samples. This is expected, as the impact of counting statistics decreases with increasing signal brightness (Duller et al., 2000).

4.3. Overdispersion variability in recovered doses

It has been shown that even under the controlled laboratory conditions of dose recovery tests, whereby all extrinsic factors can be excluded, σ_{OD} values of 7 – 12 % are nevertheless observed in single grain dose distributions (Jacobs et al., 2006; Reimann et al., 2012; Thomsen et al., 2005). This intrinsic σ_{OD} is caused by luminescence characteristics inherent within sand grains from a sample.

We calculated the σ_{OD} values for each single grain dose recovery test. The results, together with the σ_{OD} values from the natural D_es, are plotted in Figure 3c (see also Table 1). The behaviour of the Australian material (LM) and sample L-EVA-1221 (TQ I) differs from the other Moroccan samples by consistently revealing intrinsic σ_{OD} values of ∼10 % when administered doses are small, and substantially increased σ_{OD} values of up to 35 % following larger given doses.

For samples L-EVA-1083 (Rhafas) and L-EVA-1218 (TQ I), σ_{OD} values of 5-10 % (Table 1) are observed for almost all dose recovery test parameters. This is consistent with intrinsic σ_{OD} values reported in previous studies. A remarkable increase in σ_{OD}, however, can be observed for L-EVA-1083 when a small dose was given after sunlight bleaching (22 %), for L-EVA-1218 when a high administered dose was combined with green laser stimulation (19 %), and for both samples when high given doses and SOL2 were used (25 – 27 %).

Applying SOL2 stimulation prior to a high given dose results in the highest σ_{OD} (19 – 35 %) in all samples, except L-EVA-1010 (LM). For the sake of completeness, it should be noted that for sample L-EVA-1012 (LM) the intrinsic σ_{OD} following green laser (25 %) and SOL2 bleaching (35 %) at

high given doses exceeds the value determined from the natural D_e (24 %, Fig. 3c). Those values are, however, not entirely comparable, since the given dose (185 Gy) is considerably higher than the natural D_e estimate (∼21 Gy) and, therefore, intersection of the sensitivity-corrected natural signal of the individual grains occurs along different parts of the dose response curves. Intrinsic σ_{OD} after sunlight stimulation of the material prior to a high given dose (12 %) is entirely comparable to the σ_{OD} obtained for all bleaching treatments and small administered doses (6 – 11 %).

Given the highly variable results of our dose recovery experiments, we cannot confidently specify the proportion of intrinsic σ_{OD} within the natural D_e σ_{OD} for most samples. Comparisons of the internal σ_{OD} from the dose recovery experiments close to the expected natural D_es with the measured σ_{OD} from the natural D_es of each sample indicate that considerable proportions of the σ_{OD} value are caused by extrinsic factors. As neither post depositional mixing, nor incomplete bleaching is likely for any of our samples (Doerschner et al., in revision; Fitzsimmons et al., 2014; Rhodes et al., 2006), high extrinsic σ_{OD} most likely results from heterogeneous dose rates (Lomax et al., 2007). Autoradiography was undertaken at the University of Bern to verify this assumption by highlighting spatially resolved radiation inhomogeneities in our samples following the procedure described in Rufer & Preusser (2009). Autoradiographs are shown in Figure S3; high-radiation emitters are visible as black hotspots and indicate dose rate heterogeneity, thereby explaining the high values obtained for external σ_{OD}. Furthermore, visual inspection under a microscope indicates that carbonate shielding of quartz grains, which could introduce further variation in microdosimetry by reducing the dose rate received by individual grains (Olley et al., 1997), might additionally affect L-EVA-1083 (Rhafas). This effect is, however, absent from LM and TQ I samples.

5. Discussion

5.1. Dose recovery and overdispersion

In this study the dose recovery characteristics of single quartz grains of archaeological samples from two Moroccan (Rhafas and TQ I) and one Australian (LM) site were examined.

The Australian samples consist of highly sensitized, bright quartz grains which are able to recover a small laboratory given dose (close to their natural D_e) within 6 % of unity and homogeneously (σ_{OD} 6 – 11 %) over a large number of individual grains. By contrast, when administered doses are high (185 Gy), the total number of single grains passing rejection criteria decreases (Table 1), while σ_{OD} increases (12 – 35 %) and the measured/given dose ratio is systematically underestimated by up to 33 %.

For the Moroccan samples, the results are variable. The samples originate from two cave sites and consist of individual quartz grains significantly less bright than the Australian samples. These results suggest that the Moroccan material underwent comparatively fewer sensitization cycles (cycles of dose and light exposure) than the Australian samples (Moska & Murray, 2006; Pietsch et al., 2008). Dose recovery ratios and σ_{OD} values in sample L-EVA-1083 (Rhafas) and L-EVA-1218 (TQ I) are highly variable (Fig. 3). Single grains from these samples recover low administered doses with similar accuracy (1 – 17 %) and precision (σ_{OD} 5 – 22 %) as high doses (within 6 – 25 % of unity, σ_{OD} 6-27 %). They also do not show significant dependency on the bleaching treatment. Therefore, it seems most likely that the results reflect a sample-specific response to the chosen dose recovery test parameters (bleaching type and size of administered dose).

For sample L-EVA-1221 (TQ I), however, measured/given dose ratios and σ_{OD} values are clearly dependent on the magnitude of the given dose. Consequently, our results suggest that the SAR protocol would have to be declared as unsuitable for dating sample L-EVA-1221, in the case where a standard dose recovery test with a given dose close to the expected natural D_e (205 Gy) is applied. L-EVA-1221, however, passes a SAR suitability check when applied doses are low (20 Gy). Interestingly, L-EVA-1218 (TQ I) and L-EVA-1083 (Rhafas) pass standard SAR suitability checks when green laser bleaching is applied, yet fail after sunlight or SOL2 treatment, when given doses are close to their expected natural D_e (180 and 208 Gy, respectively).

Our contradictory results raise questions as to the validity of dose recovery tests in general, and more particularly as to the adequate choice of test parameters to interrogate the suitability of the SAR protocol. The Moroccan material is in general less sensitive than the Australian samples. While single grain signal intensity in all samples correlates positively with accuracy of measured/given ratio when given doses are small, even bright grains are not necessarily able to reproduce a given dose $>$ 180 Gy with any accuracy. The observed variability in intrinsic σ_{OD} in our samples is alarming, particularly when considering that the correct assessment of natural σ_{OD} is critical for reliable age determination. Underestimation of the intrinsic, and thereby overestimation of the extrinsic, σ_{OD} might result in misinterpretation of single grain dose distributions and/or selection of inappropriate statistical age models. Autoradiographs suggest that increased values of extrinsic σ_{OD} in all samples result from variations in their microdosimetry.

5.2. Single grain rejection criteria

Application of single grain rejection criteria significantly reduces the amount of acceptable grains in each dose recovery experiment presented in this study. The justification of single grain standard rejection criteria (recycling, IR depletion and recuperation) has been recently questioned in several studies (e.g. Geach et al. 2015; Guérin et al. 2015; Thomsen et al. 2012; Zhao et al. 2015. Thomsen et al. (2016) reported that standard rejection criteria for single grains "do not result in significant changes in either dose or overdispersion of the single grain distributions" in the samples that they investigated. To investigate the impact of the chosen single

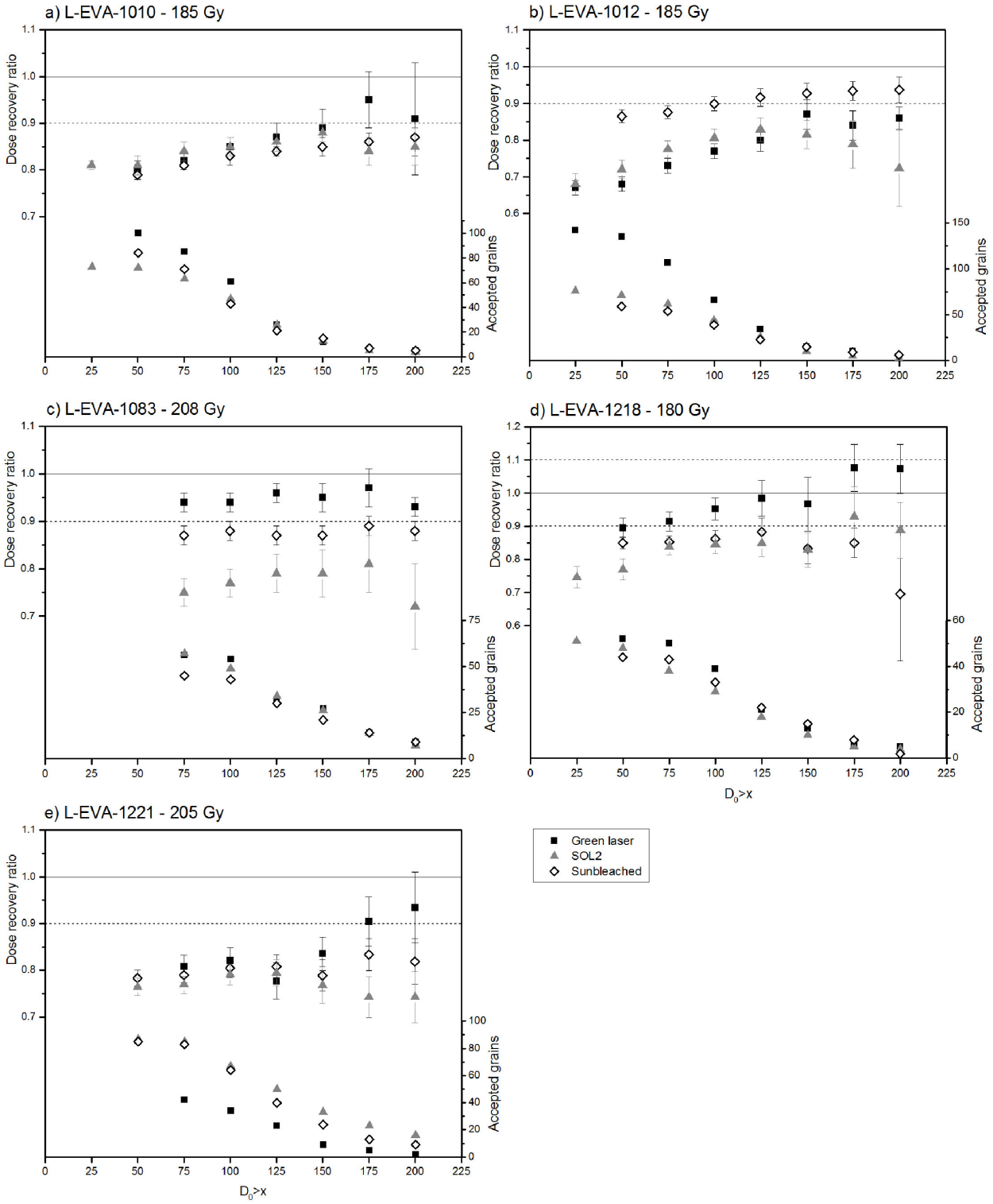

Figure 4. Dose recovery ratio and total amount of accepted grains as a function of single grain D_0 values in dose recovery experiments, with high given doses for each sample in this study.

grain rejection criteria in our dose recovery experiments, we compared dose recovery ratios and σ_{OD} values both before and after application of single grain rejection criteria (Table 1 and Table S3). The dose recovery ratios prior and subsequent to application of rejection criteria are – with the exception of L-EVA-1218 following green laser bleaching and a low given dose – indistinguishable from one another within the given error ranges. σ_{OD} values, however, were reduced considerably (up to 12 %) following application of rejection criteria in 15 out of the 30 dose recovery experiments. We, therefore,

argue that rejection of individual grains due to the chosen criteria reduces σ_{OD} values significantly in our experiments.

We further investigated the impact of applying the $D_e > 2D_0$ and the D_e error $< 30\,\%$ criteria in our samples. We undertook this exercise in response to the argument that those criteria are more likely to reject individual grains with high dose estimates rather than low dose estimates, and may consequently bias our single grain dose distributions toward underestimated dose recovery ratios and reduced σ_{OD} values. We calculated dose recovery ratios and σ_{OD} for each experiment in this study using all rejection criteria listed in Section 3, with the exception of $D_e > 2D_0$ and D_e error $< 30\,\%$ (Table S4). Our results from this exercise indicate that application of those two rejection criteria has no significant impact on dose recovery ratios and σ_{OD} values, in 29 out of 30 experiments. Only in sample L-EVA-1083 following green laser bleaching and a high given dose, do dose recovery ratios improve and σ_{OD} is significantly reduced. We then compared dose recovery test results prior to application of rejection criteria (Table S3), with results when all rejection criteria, except the $D_e > 2D_0$ and the D_e error $< 30\,\%$ were applied (Table S4). This comparative exercise shows that σ_{OD} values are still significantly reduced for 14 out of 30 dose recovery experiments, and for only one dose recovery ratio. Our findings suggest that there is no clear justification for the assumption that application of $D_e > 2D_0$ and D_e error $< 30\,\%$ criteria bias single grain dose distributions in our samples. Furthermore, our results also do not indicate that those two rejection criteria cause the apparent reduction of σ_{OD} observed prior and subsequent to application of rejection criteria – at least in the case of the samples analysed in this study.

5.3. Bleaching methods

The impact of different bleaching methods on the dose recovery characteristics of individual grains is almost negligible when given doses are small (Fig. 3, Table 1). With the exception of L-EVA-1083 following sunlight bleaching, all measured/given ratios lie within unity and σ_{OD} ranges from $5-11\,\%$. It is, however, interesting to note that a combination of green laser stimulation and low given doses consistently yields the highest proportions of acceptable grains in all samples.

When given doses exceed 180 Gy in the dose recovery experiments, variability in dose recovery ratios and σ_{OD} increases substantially compared to results following low administered doses. No obvious pattern can be observed when comparing results following sunlight and green laser bleaching, leading to the conclusion that there is most likely an additional factor influencing dose recovery results that is best described as a sample-specific response to dose recovery test parameters. This assumption is supported by the fact that both the proportion of accepted single grains, as well as the specific rejection criteria, show dependency on the sampling location.

SOL2 bleaching results – with the exception of L-EVA-1010 – considerably underestimate dose recovery ratios ($25-32\,\%$) and oversee a substantial increase in σ_{OD} ($19-35\,\%$) for all samples. In their study, Choi et al. (2009) observed an underestimation of the given dose ($10-150$ Gy) by $\sim 20\,\%$ after SOL2 treatment (> 1 h) as a consequence of sensitisation of the quartz signal during or after the first OSL measurement. Although we chose a relatively short SOL2 stimulation time (5 min) in our experiments, and sample L-EVA-1010 seemed not to be affected at all, we cannot rule out that sensitisation of the material might have taken place either during bleaching treatment or preheating prior to the first OSL signal measurement.

5.4. Administered dose

In our experiments, the most conspicuous factor driving dose recovery characteristics and especially σ_{OD} is the size of the administered dose, as has previously been argued by Thomsen et al. (2012). Determined measured/given ratios and their associated σ_{OD} in three out of five samples are undeniably dependent on the given dose, as is the oversaturation criterion for rejection of single grains.

Thomsen et al. (2016) showed that the dependency of dose recovery ratio and σ_{OD} on the administered dose can be eliminated in dose recovery experiments (with given doses > 30 Gy) by excluding individual grains with D_0 values greater or equal the given dose. They argue that underestimation of dose recovery ratio is related to the inclusion of grains with comparatively small D_0 values, and that by applying the D_0 selection criterion one is likely to discard saturated grains that might otherwise bias dose recovery test results. Following the procedure described in Thomsen et al. (2016), we plotted dose recovery ratios for our experiments with high given doses (> 180 Gy) as a function of $x > D_0$, with x ranging from $0-200$ Gy (Fig. 4, Table S5). In addition, we show the total amount of accepted grains that pass all rejection criteria for each $x > D_0$. Our observations are similar to those made by Thomsen et al. (2016); dose recovery ratios generally increase with increasing D_0 value. At a threshold value of $D_0 > 125-175$ Gy (depending on the sample), however, dose recovery ratios appear to decrease. This is probably linked to the small quantity of individual grains passing D_0 rejection criterion > 125 Gy (Table S5), which may be too few to allow reliable statistical age modelling. Although both dose recovery ratios and σ_{OD} improve in most of our experiments when the D_0 exceeds the given dose criterion is applied (Thomsen et al., 2016), the dose recovery ratios falling closest to unity in most of our samples occurred when $D_0 > 125-175$ Gy. This is the case even though not all recovery ratios lie close to unity, as was shown by Thomsen et al. (2016). The total amount of accepted grains from our samples are, however, significantly reduced to fewer than 15 grains (for 10 out of 15 experiments). Thus, we conclude that while rejection of individual grains based on their D_0 values can significantly improve dose recovery ratios and the associated σ_{OD}, it also reduces the quantity of accepted grains overall. This might present problems for statistical age modelling.

6. Conclusion

Our results demonstrate that while the main driving factor influencing beta dose recovery test ratios and σ_{OD} on single quartz grains is the size of the administered dose, sample-specific responses to chosen test parameters (size of the given dose, bleaching type) can also significantly alter the obtained results. High variability in dose recovery test results was observed that is unlikely to be derived solely from the size of the administered dose, particularly for the less sensitized Moroccan samples. Therefore, caution is advised when performing dose recovery tests on samples which are likely to have undergone relatively few sensitization cycles. We conclude that further studies are required to improve our understanding of the range of effects that irradiation time and laboratory bleaching method might have on individual samples.

Acknowledgments

This research was funded by the Max Planck Institute for Evolutionary Anthropology. The Moroccan samples were collected with the assistance of our project partners, Abdeljalil Bouzouggar, Jean-Paul Raynal and Abderrahim Mohib. Research on the Australian samples was undertaken with the permission of the Elders' Council and the Technical and Scientific Advisory Committee of the Willandra Lakes Region World Heritage Area (WLRWHA); sampling was funded by an Australian Research Council (ARC) Discovery Project (DP1092966) and assisted in the field by the project's Cultural Heritage Officer, Daryl Pappin. The authors wish to thank Steffi Hesse for her support during sample preparation and OSL measurements in the laboratory, and Daniel Rufer from the University of Bern for performing the autoradiography. The constructive comments of Kristina Thomsen substantially improved the paper.

References

Aitken, M. J. and Smith, B. W. *Optical dating: Recuperation after bleaching*. Quaternary Science Reviews, 7(34): 387–393, 1988. doi: http://dx.doi.org/10.1016/0277-3791(88)90034-0.

Arnold, L. J. and Demuro, M. *Insights into TT-OSL signal stability from single-grain analyses of known-age deposits at Atapuerca, Spain*. Quaternary Geochronology, 2015. doi: http://dx.doi.org/10.1016/j.quageo.2015.02.005.

Ballarini, M., Wallinga, J., Wintle, A. G., and Bos, A. J. J. *A modified SAR protocol for optical dating of individual grains from young quartz samples*. Radiation Measurements, 42(3): 360–369, 2007. doi: http://dx.doi.org/10.1016/j.radmeas.2006.12.016.

Bøtter-Jensen, L., Bulur, E., Duller, G. A. T., and Murray, A. S. *Advances in luminescence instrument systems*. Radiation Measurements, 32(56): 523–528, 2000. doi: http://dx.doi.org/10.1016/S1350-4487(00)00039-1.

Bøtter-Jensen, L., Andersen, C. E., Duller, G. A. T., and Murray, A. S. *Developments in radiation, stimulation and observation facilities in luminescence measurements*. Radiation Measurements, 37(45): 535–541, 2003. doi: http://dx.doi.org/10.1016/S1350-4487(03)00020-9.

Bøtter-Jensen, L. *Luminescence techniques: instrumentation and methods*. Radiation Measurements, 27(56): 749–768, 1997. doi: http://dx.doi.org/10.1016/S1350-4487(97)00206-0.

Bulur, E. *An alternative technique for optically stimulated luminescence (OSL) experiment*. Radiation Measurements, 26(5): 701–709, 1996. doi: http://dx.doi.org/10.1016/S1350-4487(97)82884-3.

Choi, J. H., Murray, A. S., Cheong, C. S., and Hong, S. C. *The dependence of dose recovery experiments on the bleaching of natural quartz OSL using different light sources*. Radiation Measurements, 44(56): 600–605, 2009. doi: http://dx.doi.org/10.1016/j.radmeas.2009.02.018.

Cunningham, A. C. and Wallinga, J. *Optically stimulated luminescence dating of young quartz using the fast component*. Radiation Measurements, 44(56): 423–428, 2009. doi: http://dx.doi.org/10.1016/j.radmeas.2009.02.014.

Demuro, M., Froese, D. G., Arnold, L. J., and Roberts, R. G. *Single-grain OSL dating of glaciofluvial quartz constrains Reid glaciation in NW Canada to MIS 6*. Quaternary Research, 77(2): 305–316, 2012. doi: http://dx.doi.org/10.1016/j.yqres.2011.11.009.

Doerschner, N., Fitzsimmons, K. E., Ditchfield, P., McLaren, S. J., Steele, T. E., Zielhofer, C., McPherron, S. P., Bouzouggar, A., and Hublin, J.-J. *A new chronology for Rhafas, northeast Morocco, spanning the North African Middle Stone Age through to the Neolithic*. PLoS ONE, in revision.

Duller, G. A. T., Bøtter-Jensen, L., and Murray, A. S. *Optical dating of single sand-sized grains of quartz: sources of variability*. Radiation Measurements, 32(56): 453–457, 2000. doi: http://dx.doi.org/10.1016/S1350-4487(00)00055-X.

Duller, G. *Distinguishing quartz and feldspar in single grain luminescence measurements*. Radiation Measurements, 37: 161–165, 2003.

Duller, G. A., Bøtter-Jensen, L., Murray, A. S., and Truscott, A. J. *Single grain laser luminescence (SGLL) measurements using a novel automated reader*. Nuclear Instruments and Methods in Physics Research BNuclear Instruments and Methods in Physics Research B, 155: 506–514, 1999.

Fitzsimmons, K. E. *An assessment of the luminescence sensitivity of Australian quartz with respect to sediment history*. Geochronometria, 38(3): 199–208, 2011. doi: 10.2478/s13386-011-0030-9.

Fitzsimmons, K. E., Stern, N., and Murray-Wallace, C. V. *Depositional history and archaeology of the central Lake Mungo lunette, Willandra Lakes, southeast Australia*. Journal of Archaeological Science, 41: 349–364, 2014. doi: http://dx.doi.org/10.1016/j.jas.2013.08.004.

Galbraith, R. F., Roberts, R. G., Laslett, G. M., Yoshida, H., and Olley, J. M. *Optical dating of single and multiple grains of quartz*

from Jinmium rock shelter, northern Australia: Part I, experimental design and statistical models. Archaeometry, 41(2): 339–364, 1999. doi: 10.1111/j.1475-4754.1999.tb00987.x.

Geach, M. R., Thomsen, K. J., Buylaert, J. P., Murray, A. S., Mather, A. E., Telfer, M. W., and Stokes, M. *Single-grain and multi-grain OSL dating of river terrace sediments in the Tabernas Basin, SE Spain.* Quaternary Geochronology, 30: 213–218, 2015.

Grubbs, F. E. *Sample Criteria for Testing Outlying Observations*. pp. 27–58, 1950. doi: 10.1214/aoms/1177729885.

Guérin, G., Combés, B., Lahaye, C., Thomsen, K. J., Tribolo, C., Urbanova, P., Guibert, P., Mercier, N., and Valladas, H. *Testing the accuracy of a Bayesian central-dose model for single-grain OSL, using known-age samples*. Radiation Measurements, 81: 62–70, 2015. doi: http://dx.doi.org/10.1016/j.radmeas.2015.04.002.

Jacobs, Z., Duller, G. A., and Wintle, A. G. *Interpretation of single grainDe distributions and calculation of De*. Radiation Measurements, 41: 264–277, 2006.

Jacobs, Z., Roberts, R. G., Galbraith, R. F., Deacon, H. J., Grn, R., Mackay, A., Mitchell, P., Vogelsang, R., and Wadley, L. *Ages for the Middle Stone Age of Southern Africa: Implications for Human Behavior and Dispersal*. Science, 332: 733–735, 2008.

Jacobs, Z., Roberts, R. G., Nespoulet, R., El Hajraoui, M. A., and Debnath, A. *Single-grain OSL chronologies for Middle Palaeolithic deposits at El Mnasra and El Harhoura 2, Morocco: Implications for Late Pleistocene humaneenvironment interactions along the Atlantic coast of northwest Africa*. Journal of Human Evolution, 62: 377–394, 2012.

Kang, S. G., Wang, X. L., and Lu, Y. C. *The estimation of basic experimental parameters in the fine-grained quartz multiple-aliquot regenerative-dose OSL dating of Chinese loess*. Radiation Measurements, 47(9): 674–681, 2012. doi: http://dx.doi.org/10.1016/j.radmeas.2012.01.009.

Li, S.-H. and Wintle, A. G. *Luminescence sensitivity change due to bleaching of sediments*. Radiation Measurements, 20(4): 567–573, 1992. doi: http://dx.doi.org/10.1016/1359-0189(92)90006-H.

Li, S.-H. and Wintle, A. G. *Sensitivity changes of luminescence signals from colluvial sediments after different bleachung procedures*. Ancient TL, 9(3): 50–53, 1991.

Lomax, J., Hilgers, A., Twidale, C. R., Bourne, J. A., and Radtke, U. *Treatment of broad palaeodose distributions in OSL dating of dune sands from the western Murray Basin, South Australia*. Quaternary Geochronology, 2(14): 51–56, 2007. doi: http://dx.doi.org/10.1016/j.quageo.2006.05.015.

Mercier, N., Wengler, L., Valladas, H., Joron, J.-L., Froget, L., and Reyss, J. *The Rhafas Cave (Morocco): Chronology of the mousterian and aterian archaeological occupations and their implications for Quaternary geochronology based on luminescence (TL/OSL) age determinations*. Quaternary Geochronology, 2: 309–313, 2007.

Moska, P. and Murray, A. S. *Stability of the quartz fast-component in insensitive samples*. Radiation Measurements, 41(78): 878–885, 2006. doi: http://dx.doi.org/10.1016/j.radmeas.2006.06.005.

Murray, A. S. and Wintle, A. G. *Luminescence dating of quartz using an improved single-aliquot regenerative-dose protocol*. Radiation Measurements, 32(1): 57–73, 2000. doi: http://dx.doi.org/10.1016/S1350-4487(99)00253-X.

Murray, A. S. and Wintle, A. G. *The single aliquot regenerative dose protocol: potential for improvements in reliability*. Radiation Measurements, 37(45): 377–381, 2003. doi: http://dx.doi.org/10.1016/S1350-4487(03)00053-2.

Olley, J. M., Roberts, R. G., and Murray, A. S. *Disequilibria in the uranium decay series in sedimentary deposits at Allen's cave, nullarbor plain, Australia: Implications for dose rate determinations*. Radiation Measurements, 27(2): 433–443, 1997. doi: http://dx.doi.org/10.1016/S1350-4487(96)00114-X.

Pietsch, T. J., Olley, J. M., and Nanson, G. C. *Fluvial transport as a natural luminescence sensitiser of quartz*. Quaternary Geochronology, 3(4): 365–376, 2008. doi: http://dx.doi.org/10.1016/j.quageo.2007.12.005.

Reimann, T., Lindhorst, S., Thomsen, K. J., Murray, A. S., and Frechen, M. *OSL dating of mixed coastal sediment (Sylt, German Bight, North Sea)*. Quaternary Geochronology, 11(0): 52–67, 2012. doi: http://dx.doi.org/10.1016/j.quageo.2012.04.006.

Rhodes, E. J., Singarayer, J., Raynal, J.-P., Westaway, K., and Sbihi-Alaoui, F. *New age estimates for the Palaeolithic assemblages and Pleistocene succession of Casablanca, Morocco*. Quaternary Science Reviews, 25: 2569–2585, 2006.

Rufer, D. and Preusser, F. *Potential of autoradiography to detect spatially resolved radiation patterns in the context of trapped charge dating*. Geochronometria, 34: 1–13, 2009.

Thomsen, K. J., Murray, A. S., Buylaert, J. P., Jain, M., Hansen, J. H., and Aubry, T. *Testing single-grain quartz OSL methods using sediment samples with independent age control from the Bordes-Fitte rockshelter (Roches d'Abilly site, Central France)*. Quaternary Geochronology, 31: 77–96, 2016. doi: http://dx.doi.org/10.1016/j.quageo.2015.11.002.

Thomsen, K. J., Murray, A. S., and Bøtter-Jensen, L. *Sources of variability in OSL dose measurements using single grains of quartz*. Radiation Measurements, 39: 47–61, 2005.

Thomsen, K. J., Murray, A. S., Bøtter-Jensen, L., and Kinahan, J. *Determination of burial dose in incompletely bleached fluvial samples using single grains of quartz*. Radiation Measurements, 42: 370–379, 2007.

Thomsen, K. J., Murray, A., and Jain, M. *The dose dependency of the over-dispersion of quartz OSL single grain dose distributions*. Radiation Measurements, 47: 732–739, 2012.

Wang, X. L., Wintle, A. G., Du, J. H., Kang, S. G., and Lu, Y. C. *Recovering laboratory doses using fine-grained quartz from Chinese loess*. Radiation Measurements, 46(10): 1073–1081, 2011. doi: http://dx.doi.org/10.1016/j.radmeas.2011.07.022.

Wengler, L. *Cultures prhistoriques et formations quaternaires au Maroc oriental. Relations entre comportements et paloenvironments au Palolithique moyen*. Thesis, 1993.

Wintle, A. and Murray, A. *A review of quartz optically stimulated luminescence characteristics and their relevance in single-aliquot regeneration dating protocols*. Radiation Measurements, 41: 369–391, 2006.

Zhao, Q. Y., Thomsen, K. J., Murray, A. S., Wei, M. J., Pan, B. L., Zhou, R., Zhao, X. H., and Chen, H. Y. *Quartz single-grain OSL dating of debris flow deposits from Miyun, north east Beijing in China.* Quaternary Geochronology, 30: 320–327, 2015.

Reviewer

Kristina Thomsen

Thesis Abstracts

Index

Sahar al Khasawneh	p. 26
Lukas Bickel	p. 26
Adelphine Bonneau	p. 27
Kathleen Rodrigues	p. 28
Shuang-li Tang	p. 28
Anil Kumar Tyagi	p. 29
Petra Urbanová	p. 30
Jingran Zhang	p. 30

Sahar al Khasawneh

Testing the New Applications of Luminescence Dating in Archaeology

December 2015

Institute of Ancient Near Eastern Archaeology, Berlin, Germany

Degree: Ph.D.

Supervisors: Dominik Bonatz, Andrew Murray

With recent major improvements in luminescence dating resulting from new developments in methodology and instrumentation, luminescence dating has become a much more powerful chronometric tool. These new developments have been widely used in geological applications, but there are very few publications testing their applicability in archaeology. This study aims to test the applicability of two major new techniques in luminescence dating to archaeological problems. In the first part, we report the first application of using the stable infrared stimulated luminescence signal measured at elevated temperature (290°C) to pottery samples from Pella, Jordan. The average Optically Stimulated Luminescence (OSL) age is 2850 $\pm$ 220 years (n=35), with the overall uncertainty dominated by systematic uncertainties; this agrees well with the range of ^{14}C ages of 2970 to 3270 cal. years BP for the same destruction horizon.

The method is also applied to the dating of young heated artefacts from three different archaeological sites in Denmark, one from the early Pre-Roman Iron Age 200 BC to AD 100, and two from the Viking period between AD 800 and 1200. No previous radiometric dating has been reported for these sites. Quartz OSL ages were derived to support the archaeological associations, and compared to the new feldspar ages. On average, there may be a small overestimation of feldspar ages compared to those from quartz, but if so it is only of significance for the heated stone samples.

The second part of the research investigated the application of OSL dating to sediment deposition in the arid zone directly resulting from human activities (well digging and construction of irrigation channels). Quartz and feldspar luminescence signals were both measured to provide two estimates of luminescence ages, and both ages are in agreement with each other, and with the archaeological assumption of the site age.

In the last part, a very recently developed technique, rock-surface dating, was applied to a three rocks sampled from the Jibal al-Gadiwiyt kite structure in southern Jordan. By examining the resetting of OSL with depth and time, this approach was able to provide detailed information about the burial and light-exposure history of the rock. The derived construction and burial ages (based on rock-surface dating but confirmed by sediment dating) are 10,000 years; considerably older than the archaeologically assumed age of 6000 years.

By using a variety of archaeological sites, this study demonstrates the immediate usefulness and future potential of recent developments in OSL dating. The accuracy of these and other luminescence dating methods, and the ability of luminescence to date otherwise undateable material, opens up many new and exciting opportunities in archaeology for the future.

Lukas Bickel

Luminescence dating of Middle Pleistocene glaciofluvial sediments of the Austrian Northern Alpine Foreland

March 2016

Institute of Applied Geology, University of Natural Resources and Life Sciences, Vienna

Degree: Dr. nat. techn.

Supervisors: Markus Fiebig, Christopher Lüthgens, Johanna Lomax

In the beginning of the 20th century, Albrecht Penck & Eduard Brckner (1901/1909) developed the concept of four large scale Quaternary alpine glaciations extending into the alpine foreland. Since then, the Northern Alpine Foreland (NAF) has played a major role in the investigation of glacial and furthermore paleo-climatic events. However, a numerical chronology has as yet not been established. This study focuses on dating the glaciofluvial deposits attributed to the penultimate glaciation (parallelized with MIS 6 in Austrian geological maps) when vast areas of the inner Alps were glaciated. In the easternmost part of the north draining valleys of the Alps, the glaciers did not reach the foreland, but formed valley glaciers confined by the mountainous terrain. Samples for luminescence dating purposes were taken from glaciofluvial sediments mainly deposited in the form of river terraces in the alpine foreland. A total of 24 samples from

5 catchment areas (from East to West Ybbs, Enns, Steyr, Krems, and Traun) were analysed within this study.

A highly dynamic depositional environment, such as a glacier-fed river system, implies the possibility of incomplete resetting of the luminescence signal in particular when transport distances are short. In an environment like this, quartz is the mineral of choice over feldspar, especially if dose rates are low and theoretically allow gaining quartz ages beyond 150 ka. However, detailed analyses of the quartz OSL signal characteristics had revealed the presence of a thermally unstable medium component in some samples. Because of the lack of independent age control, it remained unclear whether this medium component may result in significant age underestimation for affected samples. Therefore, the luminescence properties of coarse grain feldspar were analysed and revealed a general suitability for luminescence dating purposes. To obtain reliable age estimates for the samples, three luminescence signals were investigated for each sample: blue stimulated quartz OSL, infrared stimulated feldspar luminescence at 50°C (IRSL) and at an elevated temperature of 225°C (pIRIR).

Using a comparative dating approach, it was possible to establish a reliable chronology for the glaciofluvial deposits attributed to the penultimate glaciation in the NAF. A temporal correlation between the marine isotope stage 6 and the deposits of the penultimate glaciation in the NAF could hence be scientifically proven. For the first time it was possible to establish a methodologic and stratigraphic coherent age determination of the formation of terrace sediments during the penultimate glaciation in the Austrian NAF. Additionally, in comparison with previous studies from other alpine regions it was possible to show, that the transition between glacial and interglacial conditions happened relatively fast in late MIS6 / starting MIS5.

Adelphine Bonneau

Direct dating of rock art using radiocarbon and optically stimulated luminescence: the case study of southern Africa and the Canadian Shield

May 2016

Laboratoire Lux/Géotop, Département des Sciences de la Terre et de l'atmosphère, Université du Québec à Montréal, Montreal, Canada

Degree: Ph.D.

Supervisors: Prof. Michel Lamothe, Prof. Daniel Arsenault, Prof. Thomas Higham

Rock art exists all around the word. It is thought to be one of the most ancient expressions of the human mind. The artist, who created these paintings, opens a window into its world and gives the viewer a unique insight into its motivation and inspiration. Over the last 20 years or so, developments in the application of chemical, physical and geological methods have made it possible to recover the recipes used by ancient painters as well as to determine the age of the art itself. The interpretation of ancient rock art from around the world has been considerably aided by the acquisition of such data. However, there is still much to do. Palaeolithic rock art in Europe and Australia were the main beneficiaries of these developments. In other parts of the world, such as southern Africa and Canada, few dates have been obtained, and little in the way of paint characterisation studies exists.

This Ph.D. project explores direct dating of rock art from sites in southern Africa and in the Canadian Shield, using radiocarbon and optically stimulated luminescence. It introduces a new preliminary detailed characterisation of the sample to be dated, which makes it possible to select the samples which are the most likely to be successfully dated. Moreover, it reduces the necessary size of the sample. Using complementary instrumentation and methods, the characterisation results bring relative dating information if linked with superpositioning information, and where no superpositioning exists, or information is not available, they can give clues as to the composition and history of a panel or a site.

Characterisation reveals the type of carbon-based paint used, which can then be radiocarbon dated, for example, charcoal, soot, or carbon-blacks. This information is essential for understanding the age obtained. At the same time, this characterisation records the presence and estimates the proportions of radiocarbon contaminants in the samples, such as calcium oxalates, calcium carbonates and humic acids. A chemical pre-treatment can then be adapted to dissolve all the contaminants detected, checked with Fourier-Transform Infra-Red (FTIR) analysis. Using these methods, 46 dates were obtained on rock art sites from southern Africa. These include the first ever dates from rock art in Lesotho and in Botswana and constitute the largest dating project on rock art ever undertaken in this part of the world.

Optically stimulated luminescence (OSL) cannot give a definitive date for rock art, but the experiments carried out for this project proved that this technique may be applied under specific conditions: where the rock support is suitable for OSL dating, given a thick paint layer and sufficient exposure of the rock face to daylight.

In the Canadian Shield, none of the dating methods was applicable. However, the precise characterisation conducted on the paints reveals different paint recipes in the same site giving new clues to reconstruct some parts of the "chaîne opératoire" of the site.

Characterisation of paint and dates obtained in this project make it possible to start developing a dialogue between the archaeological record of hunter-gatherer activity preserved in paint and that preserved in occupational deposits.

A PDF of this thesis can be downloaded from: http://www.archipel.uqam.ca/

Kathleen Rodrigues

OSL dating of a coastal Swift Creek occupation at Harrison Ring, Bay County, Florida

September 2015

McMaster University, Hamilton, Canada

Degree: M.Sc.
Supervisor: W.J. Rink

A total of 17 samples were collected for OSL dating from a Swift Creek archaeological site, known as Harrison Ring, which lies on the Tyndall Air force peninsula in northwest Florida. High-resolution vertical sampling conducted at 10 cm intervals from the surface was performed in order to determine the timing of occupation at the site, and to look for patterns in radiation dosimetry and post-depositional disturbance that can compromise OSL results. We find OSL ages determined using both 0.5 mm aliquots and single grains at the archaeological levels (approximately 1751 ± 339 years ago) to be consistent with the timing of early Swift Creek cultures on the Florida Gulf Coast. The ages we report are both consistent with radiocarbon dates taken at Harrison Ring, and those taken at other Swift Creek sites on the Gulf Coast. In general, we find OSL equivalent doses that show high overdispersion and skewness that we attribute to beta-microdosimetry and possible bioturbation in the profiles. We also present results from a test with a dosimetric technique employing $Al_2O_3 : C$ chips. By using $Al_2O_3 : C$ dosimeters, we find that large variability in beta dose rates exist in the sedimentary profile at Harrison Ring. We also show that the best agreement with independent age control at this site exists when calculating ages using a beta dose rate from NAA/DNC and gamma dose rate from $Al_2O_3 : C$ dosimetry.

A PDF of this thesis can be downloaded from: https://macsphere.mcmaster.ca/handle/11375/18378

Shuang-li Tang

Low temperature thermochronological luminescence dating study and its application to the Fugong Valley of Nujiang River and the Longyangxia Gorge of Yellow River in the eastern Tibetan Plateau

December 2015

Department of Earth Sciences, The University of Hong Kong, Hong Kong

Degree: Ph.D.
Supervisor: Sheng-hua Li

The luminescence dating method has great potential in the development of low temperature thermochronology, due to its low equivalent closure temperatures of 35-80°C. It can determine the instantaneous denudation rate and true uplift rate, which is faster than the regional exhumation rate, especially for the last 1 million years. The luminescence signal is a result of the competing effects between the trapping of electrons induced by irradiation and the decay of trapped electrons by heating. The dimensionless luminescence signals are evaluated by the equivalent dose (D_e). The D_e value corresponds to the apparent age, which is the time elapsed from the equivalent closure temperature to the present. Numerical simulation indicates that the equivalent closure temperature is dependent on the activation energy E and frequency factor s of electron traps, and the cooling rate η. Protocols of D_e determination were evaluated and improved for this thermochronological study. Single aliquot regenerative dose isothermal thermoluminescence (SAR-ITL) and the multiple aliquots regenerative dose thermoluminescence (MAR-TL) protocols were studied using quartz from rock samples collected in the Nujiang (Salween) River of Tibet, China. In the SAR-ITL protocol, temperatures of 235 and 255°C were selected for the isothermal thermoluminescence (ITL) measurement. A cutheat (preheat) to 245 and 265°C were used to remove the thermoluminescence (TL) signal from lower temperature peaks, respectively. The integral of ITL signal between 10-20 seconds was used for D_e calculation. In the MAR-TL protocol, a cutheat (preheat) of 235°C was used to remove the low temperature peaks. D_e values at temperatures of 250-290°C were used for the thermochronological study. The SAR-ITL D_e values appeared to be 40-50°C lower from D_e(T) plots of MAR-TL. It was indicated that the SAR-ITL and MAR-TL protocols were both appropriate for the thermochronological studies, and the MAR-TL was more efficient in the D_e measurement. This is because the MAR-TL protocol can measure D_e values of different TL peaks in one run. The TL signals at different heating temperatures have different thermal stabilities, and, hence, multiple thermometers of different closure temperatures can be identified from a single TL signal curve. Thus, a group of apparent ages can be obtained for a single sample in one measurement. The signals of K-feldspar were also explored in the thermochronological study because they were stronger and had better reproducibility. The TL and ITL signals were studied with different measurement procedures, including the multiple aliquots additive dose protocol (MAA), as well as MAR and SAR protocols. The MAA-TL, MAR-TL, MAA-ITL, MAR-ITL and SAR-ITL protocols were compared by measuring the natural D_e of the K-feldspar samples. The MAR-ITL protocol was not appropriate for the K-feldspar thermochronology work, because it produced a sizeable underestimation at 295°C. The MAR-TL and SAR-ITL protocols have potential to be applied in future thermochronological studies of K-feldspar. The Fugong valley of the Nujiang River and the Longyangxia Gorge of the Yellow River were selected to apply the luminescence dating method to qualify the uplift and river incision processes in the eastern margin of the Tibetan Plateau, China. The MAR-TL protocol was used in the measurement of D_e values. Quartz grains were extracted from twenty samples collected at different elevations on the valley slope. The apparent age results indicate an accelerated incision from 0.4 mm/yr at 263 ka to 18.8 mm/yr at 8 ka. This acceleration increased dramatically since 25 ka. From 263 ka to the present, the valley had been incised ~1042 m. The equivalent closure temperature based on depth of incision is 41-46°C. This was consistent with a

46°C closure temperature calculated from a numerical simulation with a incision rate of 0.4 mm/yr (0.01-0.012 °C/ka). This accelerating incision process indicates that crustal uplift was due to the uplift of the southeastern Tibetan Plateau. Assuming the river channel was at a very low elevation (e.g. 0-1000 m) at 263 ka ago, the estimated average uplift rate is ∼7.1-10.9 mm/yr. In the Longyangxia Gorge of the Yellow River, quartz grains were extracted from eight samples collected at different elevations on the gorge wall. The apparent age results indicate that the incision of Longyangxia Gorge initiated before 50.77 ka. This incision gradually accelerated from 4.87 mm/yr at 41.41 ka to 19.60 mm/yr at 7.70 ka. The estimated extent of incision into the granodiorite pluton at Longyangxia Gorge is $>$ 448.5 m during the last 50.77 ka. This indicates a continuous uplift of the northeastern Tibetan Plateau.

A PDF of this thesis can be downloaded from: http://hub.hku.hk/handle/10722/223045

Anil Kumar Tyagi

Luminescence Dating of Past Seismic and Tectonic Events: Methodological Aspects and Applications

December 2015

Gujarat University, Ahmedabad Gujarat, India

Degree: Ph.D.

Supervisor: Prof. Ashok Kumar Singhvi

Climate and tectonics are important processes that sculpt the surface of Earth and control other geomorphic and sediment transport processes. Therefore understanding of timing and amplitude of the past seismic and tectonic history of area during the geological past is needed to inform the planning of built and other infrastructures. This calls for the development of long time series of patterns and nature of release of stress as earthquakes. This thesis examined three possibilities to reconstruct the timing of the past earthquakes using both theoretical calculations from first principles and their field/laboratory validations in respect of the use of luminescence dating technique to date most recent thermal or optical exposure of sedimentary material related to earthquakes. Three possible archives of the chronology of past earth quakes are the sand dikes, the fault gouges and tectonically sculpted landforms.

Earlier studies on sand dikes indicated a reduced luminescence signal in dikes compared to host and this was despite the absence of any obvious possibility of thermal or daylight bleaching. Following recent preliminary works, this thesis examined in detail the aspect of flash heating of sediment in sand dike due to grain friction and inferred that heating up to few hundred degrees could occur during the injection of dike. Critical parameters were sediment viscosity, width of the dike and injection velocity. Effect of these parameters on rise in temperature was examined. Flash heating reconciled with thermal zeroing of luminescence signal and was validated by luminescence dating and analysis of luminescence properties of the sand dike and host samples from NorthEast (Assam). These studies suggested that resetting of luminescence due to viscous heating during injection of sand dikes, did occur. Experimental validation included the estimation of extent of heating in dike samples by laboratory measurement. For this sensitivity of 110 °C TL peak of quartz was used.

The second possibility of dating past earthquakes/tectonic event was via the dating of rock material that gets pulverized during the movement along a fault viz. the fault gouge. Heat excursion due to slip was simulated along with heat dissipation and it was seen that sufficient heat to reset luminescence can be generated for slip of about 15 cm. This can be dated using luminescence to provide a direct age of the seismic event.

The third possibility of dating tectonic events was via the dating of fault scarp and river channels affected by the earthquakes. The principal conclusion of the thesis is that flash heating under suitable conditions can result in the zeroing of luminescence. Thermal zeroing of luminescence can result in resting of signal in dike and gouge material. Conventional sediment dating using luminescence also enables constraining timing of past seismic events using material from scarps. These possibilities therefore make luminescence dating an attractive option for dating of past earth quakes and tectonic events.

In rocky terrains, catastrophic earthquakes lead to the formation of the gouge material. Extent of heating in the fault gouge material was estimated by theoretical calculations and validated with the experiments in laboratory. Attempt was also made to understand the effect of stress on the quartz grains. Quartz grains were stressed by dropping different mass from different heights and luminescence from these stressed grains were recorded. The results show the pattern of reduction in luminescence due to the applied stress on the samples.

The luminescence studies were also made using standard laboratory protocols on the dike, fault gouge and fault scarp samples to estimate the time of tectonic events. Based on the studies on sand dike samples four earthquake events of M$>$6 were identified in NorthEast Shillong. Analysis of fault gouge samples suggested two earthquakes in SikkimDarjeeling Himalaya. Fault scarp samples suggested that the present Allah bund scarp was an outcome of two major earthquakes in the area.

A PDF of this thesis can be downloaded from: http://shodhganga.inflibnet.ac.in/and from http://14.139.122.29/webopac/main.aspx

Petra Urbanová

Researches on direct dating of constructions: Investigations of the potentials of Optically Stimulating Luminiscence to date archaeological mortars

November 2015

Institut de Recherche sur les ArcheoMATeriaux (IRAMAT) UMR 5060 CNRS - Université de Bordeaux Montaigne, France

Degree: Ph.D.
Supervisor: Pierre Guibert

The presented research aims at direct dating of historical constructions, the interdisciplinary issues of which have a high significance in the field of archaeology. The objective was to put into practice a dating method dealing with mortars, a category of materials more convenient and much more representative for the chronology of buildings than brick or wood constructions that may be reused. Current attempts in mortar dating focus on the radiocarbon method which has, however, its limitations that persist despite more than forty years of applications. Thus, dating of mortars by optically stimulated luminescence (OSL), firstly mentioned in the literature in 2000, may become an interesting alternative. The basic premise in such an analysis is that quartz in the sand used for making mortar is optically zeroed during the preparation process. The moment to be dated is the last exposure of mortar to light, before being embedded within the masonry and hidden from light.

The monuments dated in this Ph.D. thesis constitute a group of reference structures from the Gallo-Roman antiquity to the Middle Ages well-dated by other independent chronological approaches. The objective is to compare the chronology obtained by OSL with the known one and thereby to proof the validity of the method. The OSL dating procedure of mortars is complicated due to numerous factors. First of all, due to the short exposure to light the optical bleaching of quartz grains in mortar is not homogeneous. In addition, the young age of the dated material (maximally 2000 years old in our case) implies signals of a weak intensity and a necessity to adapt conveniently the measurement protocol. Finally, especially the coarse-grained mortars can be affected by microdosimetric effects of high variability. All these factors are taken into account when selecting a convenient dating methodology comprising the following stages: characterization of mortar by optical microscopy, by SEM-EDX and by beta autoradiography, the measurement of individual archaeological doses by the single grain technique and the determination of the annual dose rate by low background gamma spectrometry, Al_2O_3 dosimetry and inductively coupled plasma mass spectrometry.

The study shows that archaeological mortars can be bleached during the preparation process. The individual analysis of each grain is here the only way how to get the precise information about the nature of the material studied. The work raises important methodological questions on the evaluation of single grain distributions and points out the importance of the material characterization before realizing the SG-OSL dating.

As a result of this 3-year project studying the set of 33 mortars, we are able to present today the convenient methodology for dating mortars by OSL obtaining a good agreement between OSL and reference ages for many samples. The promising potential of the method was demonstrated on undated mortars sampled during the archaeological research in the crypt of the Saint Seurin basilica, Bordeaux. This represents a step forward in the fields of archaeology and construction history.

A PDF of this thesis can be downloaded from: www.u-bordeaux-montaigne.fr (contact: urbanpetra@seznam.cz)

Jingran Zhang

Responses of Late Quaternary sediments to climate change—Luminescence dating of coastal, lacustrine and aeolian deposits from northern China and Germany

June 2016

Freie Universität Berlin, Berlin, Germany

Degree: Dr. rer. nat.
Supervisors: Prof. Dr. Manfred Frechen, Dr. Sumiko Tsukamoto

Chronology is the backbone of history. Geochronology plays the same role in geosciences research. Optically stimulated luminescence (OSL) dating is one of the most intensively and commonly applied numerical dating techniques in determining the age of Late Quaternary sediments. This dissertation focuses both on quartz OSL dating applications of various Late Quaternary sediments and on methodological development in feldspar luminescence dating. Given validation of any dating method by comparison with other methods is necessary, radiocarbon dating is carried out as independent age control whenever possible. The research samples were collected from three different sedimentary archives, which are the Garding-2 core (240 m) drilled in the Eiderstedt Peninsula from the German North Sea coast, loess in central and western Qilian Shan in northwestern China and Huangqihai Lake from the East Asian monsoon marginal area in northern China.

The quartz OSL dating using single-aliquot regenerative-dose (SAR) protocol is primarily carried out for all three case studies. For the Garding-2 core, sand-sized quartz fractions are extracted from the uppermost 26 m of the core. The luminescence performance demonstrated that the quartz OSL signals from the coastal sediments were sufficiently bleached prior to deposition. The OSL ages coupled with ^{14}C ages are proven to be reliable and robust. For the loess sediments from the central and Qilian Shan area, fine-grained quartz fractions are used to conduct OSL dating. A relatively larger uncertainty of the quartz OSL ages is observed for some of the loess samples due to their low OSL sensitivity, which is probably related to a short sedimentation history of the particles from the source region to depositional site. The routine

quartz OSL dating encounters major problems in dating the samples from Huangqihai Lake due to the chemical irremovable feldspar contamination and the samples from the deeper part of the Garding-2 core because of the quartz signal saturation. To deal with the feldspar contamination, a post-IR OSL dating protocol using pulsed stimulation is employed to discriminate against the unwanted feldspar signals. Typical quartz OSL signals are observed after pulsing indicating that the feldspar contamination can be sufficiently removed. The obtained pulsed OSL ages are generally in stratigraphic order in the geographical context and agree with independent age control from four radiocarbon ages.

By applying the suitable dating protocols of quartz OSL, the chronological frameworks of each sedimentary archive are established. The 16 ka coastal sedimentary record generated from the Garding-2 core reveals that after last deglaciation the transgression started in the early Holocene and the sea level reached the core site at around 8.3 ka and continued to rise with a decelerated rate until around 3 ka. In northern China, the OSL chronology of loess demonstrates that the deposition of dust was widespread since the last deglaciation ($\sim$13 ka) until $\sim$3.6 ka in the northern piedmont of the central and western Qilian Shan area. During the last glacial period, loess sedimentation is only sporadically and episodically registered which is dated back at least to $\sim$80 ka. The OSL ages obtained from a series of outcrops from Huangqihai Lake in northern China indicated a lake highstand during the early Holocene ($\sim$108 ka). The previously reported high lake level during MIS 3 that extensively occurred in northern and western China is not supported by the current record.

As an alternative dosimeter, feldspar has much higher saturation doses compared to quartz, which shows great potential in extending the age range of luminescence dating and thus allowing the determining of older geological events (likely back to Mid-Pleistocene). The recently developed post-IR IRSL (pIRIR) dating of feldspar at elevated temperature is tested using either sand-sized K-rich feldspar or polymineral fine grains from the Garding-2 core sediment and the Qilian Shan loess. The pIRIR and the corresponding IR50 signals are systematically investigated under various preheat and stimulation temperatures in terms of residual dose, fading rate and dose recovery measurements. Previously reported general behaviours of the pIRIR signal are confirmed, e.g. the higher preheat and stimulation temperatures are used, the higher residual and lower fading can be expected. The pIRIR dating of feldspar yields ages up to more than 400 ka without saturation, which is very promising for the investigation of the deeper part of the Garding-2 core. The pIRIR D_e plateau is observed for the polymineral fine grains from four loess samples with different ages. However, the dating implication of the pIRIR De plateau cannot be fully understood so far. Further investigations are still imperative in order to unveil the fundamental mechanisms of the pIRIR signal.

A PDF of this thesis can be downloaded from: http://www.diss.fu-berlin.de/diss/receive/FUDISS_thesis_000000101982

Bibliography

Compiled by Daniel Richter

From 1st December 2015 to 15th May 2016

Ahlborn, M., Haberzettl, T., Wang, J., Fürstenberg, S., Mäusbacher, R., Mazzocco, J., Pierson, J., Zhu, L., and Frenzel, P. (2016). Holocene lake level history of the Tangra Yumco lake system, southern-central Tibetan Plateau. *The Holocene* **26,** 176-187.

Baria, R., Cano, N. F., Silva-Carrera, B. N., Watanabe, S., Neves, E. G., Tatumi, S. H., and Munita, C. S. (2015). Archaeometric studies of ceramics from the So Paulo II archaeological site. *Journal of Radioanalytical and Nuclear Chemistry* **306,** 721-727.

Barros, L. F. d. P., Coe, H. H. G., Seixas, A. P., Magalhães Jr, A. P., and Macario, K. C. D. (2016). Paleobiogeoclimatic scenarios of the Late Quaternary inferred from fluvial deposits of the Quadrilátero Ferrífero (Southeastern Brazil). *Journal of South American Earth Sciences* **67,** 71-88.

Bateman, M. D., Evans, D. J. A., Buckland, P. C., Connell, E. R., Friend, R. J., Hartmann, D., Moxon, H., Fairburn, W. A., Panagiotakopulu, E., and Ashurst, R. A. (2015). Last glacial dynamics of the Vale of York and North Sea lobes of the British and Irish Ice Sheet. *Proceedings of the Geologists' Association* **126,** 712-730.

Bhattacharjee, D., Jain, V., Chattopadhyay, A., Biswas, R. H., and Singhvi, A. K. (2016). Geomorphic evidences and chronology of multiple neotectonic events in a cratonic area: Results from the Gavilgarh Fault Zone, central India. *Tectonophysics* **677–678,** 199-217.

Calzolari, G., Della Seta, M., Rossetti, F., Nozaem, R., Vignaroli, G., Cosentino, D., and Faccenna, C. (2016). Geomorphic signal of active faulting at the northern edge of Lut Block: Insights on the kinematic scenario of Central Iran. *Tectonics* **35,** 76-102.

Carr, A. S., Armitage, S. J., Berrío, J.-C., Bilbao, B. A., and Boom, A. (2016). An optical luminescence chronology for late Pleistocene aeolian activity in the Colombian and Venezuelan Llanos. *Quaternary Research* **85,** 299-312.

Chapot, M. S., Roberts, H. M., Duller, G. A. T., and Lai, Z. P. (2016). Natural and laboratory TT-OSL dose response curves: Testing the lifetime of the TT-OSL signal in nature. *Radiation Measurements* **85,** 41-50.

Chaussé, C., Blaser, F., Debenham, N., Roque, C., and Vartanian, E. (2015). Pléistocène supérieur et paléolithique dans le domaine des sables stampiens (rupéliens) du sud du bassin de Paris: les données du site de Melun-Montaigu(Seine-et-Marne, France). *Quaternaire* **26,** 245-255.

Chen, R., Pagonis, V., and Lawless, J. L. (2015). Time and dose-rate dependence of TL and OSL due to competition between excitation and fading. *Radiation Measurements* **82,** 115-121.

Chruścińska, A., and Kijek, N. (2016). Thermally modulated optically stimulated luminescence (TM–OSL) as a tool of trap parameter analysis. *Journal of Luminescence* **174,** 42-48.

Clemmensen, L. B., Glad, A. C., and Kroon, A. (2016). Storm flood impacts along the shores of micro-tidal inland seas: A morphological and sedimentological study of the Vesterlyng beach, the Belt Sea, Denmark. *Geomorphology* **253,** 251-261.

Costas, S., Naughton, F., Goble, R., and Renssen, H. (2016). Windiness spells in SW Europe since the last glacial maximum. *Earth and Planetary Science Letters* **436,** 82-92.

de León, D. Z., Kershaw, S., and Mahan, S. (2016). Quaternary alluvial fans of Ciudad Juárez, Chihuahua, northern México: OSL ages and implications for climatic history of the region. *Boletin de la Sociedad Geologica Mexicana* **68,** 111-128.

De Pascale, G. P., Chandler-Yates, N., Dela Pena, F., Wilson, P., May, E., Twiss, A., and Cheng, C. (2016). Active tectonics west of New Zealand's Alpine Fault: South Westland Fault Zone activity shows Australian Plate instability. *Geophysical Research Letters* **43,** 3120-3125.

Delile, H., Schmitt, L., Jacob-Rousseau, N., Grosprêtre, L., Privolt, G., and Preusser, F. (2016). Headwater valley response to climate and land use changes during the Little Ice Age in the Massif Central (Yzeron basin, France). *Geomorphology* **257,** 179-197.

Dietze, M., Dietze, E., Lomax, J., Fuchs, M., Kleber, A., and Wells, S. G. (2016). Environmental history recorded in aeolian deposits under stone pavements, Mojave Desert, USA. *Quaternary Research* **85,** 4-16.

Dietze, M., Kreutzer, S., Burow, C., Fuchs, M. C., Fischer, M., and Schmidt, C. (2016). The abanico plot: Visualising chronometric data with individual standard errors. *Quaternary Geochronology* **31,** 12-18.

Dougherty, A. J., Choi, J.-H., and Dosseto, A. (2016). Prograded Barriers plus GPR plus OSL = Insight on Coastal Change over Intermediate Spatial and Temporal Scales. *Journal of Coastal Research* **Spec.Iss. 75,** 368-372.

Druzhinina, O., Molodkov, A., Bitinas, A., Bregman, E. (2016). The Oldest Evidence for Human Habitation in the Baltic Region: A Preliminary Report on the Chronology and Archaeological Context of the Riadino-5 Archaeological Site. *Geoarchaeology: An International Journal* **31,** 156–164.

Duval, M. (2016). Comments on "ESR dating of the Majuangou and Banshan Paleolithic sites in the Nihewan Basin, North China" by Liu et al. (2014). *Journal of Human Evolution* **90,** 198-202.

Faershtein, G., Porat, N., Avni, Y., and Matmon, A. (2016). Aggradation–incision transition in arid environments at the end of the Pleistocene: An example from the Negev Highlands, southern Israel. *Geomorphology* **253,** 289-304.

Fairburn, W. A., and Bateman, M. D. (2016). A new multi-stage recession model for Proglacial Lake Humber during the retreat of the last British–Irish Ice Sheet. *Boreas* **45,** 133-151.

Fan, Y., Zhang, F., Zhang, F., Liu, W., Chen, X., Fan, T., Wang, Y., Chen, F., and Lai, Z. (2016). History and mechanisms for the expansion of the Badain Jaran Desert, northern China, since 20 ka: Geological and luminescence chronological evidence. *The Holocene* **26,** 532-548.

Fasoli, M., and Martini, M. (2016). The composite nature of the thermoluminescence UV emission of quartz. *Journal of Luminescence* **173,** 120-126.

Fattahi, M., and Walker, R. (2016). Optical dating of Holocene lake bed sediments of the Nimbluk Plain, Khorasan, Northeast Iran: Implications for the climate change and palaeo-environment. *Journal of the Earth and Space Physics* **41,** 1-12.

Frankel, K. L., Owen, L. A., Dolan, J. F., Knott, J. R., Lifton, Z. M., Finkel, R. C., and Wasklewicz, T. (2016). Timing and rates of Holocene normal faulting along the Black Mountains fault zone, Death Valley, USA. *Lithosphere* **8,** 3-22.

Gadot, Y., Davidovich, U., Avni, G., Avni, Y., Piasetzky, M., Faershtein, G., Golan, D., and Porat, N. (2016). The formation of a Mediterranean terraced landscape: Mount Eitan, Judean Highlands, Israel. *Journal of Archaeological Science: Reports* **6,** 397-417.

Gallagher, C., Telfer, M. W., and Ó Cofaigh, C. (2015). A Marine Isotope Stage 4 age for Pleistocene raised beach deposits near Fethard, southern Ireland. *Journal of Quaternary Science* **30,** 754-763.

Gao, H., Li, Z., Pan, B., Liu, F., and Liu, X. (2016). Fluvial responses to late Quaternary climate change in the Shiyang River drainage system, western China. *Geomorphology* **258,** 82-94.

Glasser, N. F., Jansson, K. N., Duller, G. A. T., Singarayer, J., Holloway, M., and Harrison, S. (2016). Glacial lake drainage in Patagonia (13-8 kyr) and response of the adjacent Pacific Ocean. *Scientific Reports* **6,** 21064.

Gliganic, L. A., Cohen, T. J., Slack, M., and Feathers, J. K. (2016). Sediment mixing in aeolian sandsheets identified and quantified using single-grain optically stimulated luminescence. *Quaternary Geochronology* **32,** 53-66.

Grellet-Tinner, G., Spooner, N. A., and Worthy, T. H. (2016). Is the "Genyornis" egg of a mihirung or another extinct bird from the Australian dreamtime? *Quaternary Science Reviews* **133,** 147-164.

Guilarte, V., Trompier, F., and Duval, M. (2016). Evaluating the Potential of Q-Band ESR Spectroscopy for Dose Reconstruction of Fossil Tooth Enamel. *Plos One* **11**, e0150346.

Guo, X., Sun, Z., Lai, Z., Lu, Y., and Li, X. (2016). Optical dating of landslide-dammed lake deposits in the upper Yellow River, Qinghai-Tibetan Plateau, China. *Quaternary International* **392,** 233-238.

Gusev, E.A., Molodkov, A.N., Streletskaya, I.D., Vasiliev, A.A., Anikina, N.Y., Bondarenko, S.A., Derevyanko, L.G., Kupriyanova, N.V., Maksimov, F.E., Polyakova, E.I., Pushina, Z.V., Stepanova, G.V., Oblogov, G.E. (2016). Deposits of the Kazantsevo Transgression (MIS 5) in the Northern Yenisei Region. *Russian Geology and Geophysics* **57,** 586–596.

Haddadchi, A., Olley, J., and Pietsch, T. (2016). Using LM-OSL of quartz to distinguish sediments derived from surface-soil and channel erosion. *Hydrological Processes* **30,** 637-647.

Han, F., Sun, C., Bahain, J.-J., Zhao, J., Lin, M., Xing, S., and Yin, G. (2016). Coupled ESR and U-series dating of fossil teeth from Yiyuan hominin site, northern China. *Quaternary International* **400,** 195-201.

Hoffecker, J. F., Holliday, V. T., Anikovich, M. V., Dudin, A. E., Platonova, N. I., Popov, V. V., Levkovskaya, G. M., Kuz'mina, I. E., Syromyatnikova, E. V., Burova, N. D., Goldberg, P., Macphail, R. I., Forman, S. L., Carter, B. J., and Crawford, L. J. (2016). Kostenki 1 and the early Upper Paleolithic of Eastern Europe. *Journal of Archaeological Science: Reports* **5,** 307-326.

Honegger, M., and Williams, M. (2015). Human occupations and environmental changes in the Nile valley during the Holocene: The case of Kerma in Upper Nubia (northern Sudan). *Quaternary Science Reviews* **130,** 141-154.

Houmark-Nielsen, M., Bennike, O., Lemdahl, G., and Lüthgens, C. (2016). Evidence of ameliorated Middle Weichselian climate and sub-arctic environment in the western Baltic region: coring lake sediments at Klintholm, Møn, Denmark. *Boreas* **45,** 347-359.

Hu, G., Huang, C. C., Zhou, Y., Pang, J., Zha, X., Guo, Y., Zhang, Y., and Zhao, X. (2016). Extreme paleoflood events 3200–3000 a BP in the Jingyuan–Jingtai reaches of the upper Yellow River, China. *The Holocene* **26,** 790-800.

Hu, X., Pan, B., Kirby, E., Gao, H., Hu, Z., Cao, B., Geng, H., Li, Q., and Zhang, G. (2015). Rates and kinematics of active shortening along the eastern Qilian Shan, China, inferred from deformed fluvial terraces. *Tectonics* **34,** 2478-2493.

Hu, Z., Pan, B., Guo, L., Vandenberghe, J., Liu, X., Wang, J., Fan, Y., Mao, J., Gao, H., and Hu, X. (2016). Rapid fluvial incision and headward erosion by the Yellow River along the Jinshaan gorge during the past 1.2 Ma as a result of tectonic extension. *Quaternary Science Reviews* **133,** 1-14.

Huckleberry, G., Ferguson, T. J., Rittenour, T., Banet, C., and Mahan, S. (2016). Identification and dating of indigenous water storage reservoirs along the Rio San José at Laguna Pueblo, western New Mexico, USA. *Journal of Arid Environments* **127,** 171-186.

Jia, L., Zhang, X., Ye, P., Zhao, X., He, Z., He, X., Zhou, Q., Li, J., Ye, M., Wang, Z., and Meng, J. (2016). Development of the alluvial and lacustrine terraces on the northern margin of the Hetao Basin, Inner Mongolia, China: Implications for the evolution of the Yellow River in the Hetao area since the late Pleistocene. *Geomorphology* **263,** 87-98.

Jones, M. D., Maher, L. A., Macdonald, D. A., Ryan, C., Rambeau, C., Black, S., and Richter, T. (2016). The environmental setting of Epipalaeolithic aggregation site Kharaneh IV. *Quaternary International* **396,** 95-104.

Kalińska-Nartiša, E., and Nartišs, M. (2016). The fan-like forms in the southern margin of the Mazovian Lowland area (Central Poland): a new high-resolution textural-timing study. *International Journal of Earth Sciences* **105,** 885-903.

Kalita, J. M., and Wary, G. (2016). Trap and recombination sites of biotite mineral estimated by thermoluminescence analysis. *Journal of Luminescence* **170, Part 1,** 64-71.

Kang, S., Roberts, H. M., Wang, X., An, Z., and Wang, M. (2015). Mass accumulation rate changes in Chinese loess during MIS 2, and asynchrony with records from Greenland ice cores and North Pacific Ocean sediments during the Last Glacial Maximum. *Aeolian Research* **19,** 251-258.

Karátson, D., Wulf, S., Veres, D., Magyari, E. K., Gertisser, R., Timar-Gabor, A., Novothny, Á., Telbisz, T., Szalai, Z., Anechitei-Deacu, V., Appelt, O., Bormann, M., Jánosi, C., Hubay, K., and Schäbitz, F. (2016). The latest explosive eruptions of Ciomadul (Csomád) volcano, East Carpathians — A tephrostratigraphic approach for the 51–29 ka BP time interval. *Journal of Volcanology and Geothermal Research* **319,** 29-51.

Karmakar, M., Bhattacharyya, S., Mazumdar, P. S., and Singh, S. D. (2015). On the determination of activation energy and the order of kinetics in thermoluminescence. *Radiation Effects and Defects in Solids* **170,** 977-988.

Kaya Keleş, Ş., Meriç, N., and Polymeris, G. S. (2016). Dose response on the 110 °C thermoluminescence peak of un-heated, synthetic Merck quartz. *Physica B: Condensed Matter* **493,** 17-24.

Kehl, M., Burow, C., Cantalejo, P., Domínguez-Bella, S., Durán, J. J., Henselowsky, F., Klasen, N., Linstädter, J., Medianero, J., Pastoors, A., Ramos, J., Reicherter, K., Schmidt, C., and Weniger, G.-C. (2016). Site formation and chronology of the new Paleolithic site Sima de Las Palomas de Teba, southern Spain. *Quaternary Research* **85,** 313-331.

King, G. E., Herman, F., Lambert, R., Valla, P. G., and Guralnik, B. (2016). Multi-OSL-thermochronometry of feldspar. *Quaternary Geochronology* **33,** 76-87.

Kitis, G., Polymeris, G. S., Şahiner, E., Meriç, N., and Pagonis, V. (2016). Influence of the infrared stimulation on the optically stimulated luminescence in four K-feldspar samples. *Journal of Luminescence* **176,** 32-39.

Kolb, T., Fuchs, M., and Zöller, L. (2016). Deciphering fluvial landscape evolution by luminescence dating of river terrace formation: A case study from Northern Bavaria, Germany. *Zeitschrift für Geomorphologie* **60,** 29-48.

Kothyari, G. C., Rastogi, B. K., Morthekai, P., and Dumka, R. K. (2016). Landform development in a zone of active Gedi Fault, Eastern Kachchh rift basin, India. *Tectonophysics* **670,** 115-126.

Kothyari, G. C., Rastogi, B. K., Morthekai, P., Dumka, R. K., and Kandregula, R. S. (2016). Active segmentation assessment of the tectonically active South Wagad Fault in Kachchh, Western Peninsular India. *Geomorphology* **253,** 491-507.

Kumar, D., Reddy, D. V., and Pandey, A. K. (2016). Paleoseismic investigations in the Kopili Fault Zone of North East India: Evidences from liquefaction chronology. *Tectonophysics* **674,** 65-75.

Küster, M., Fülling, A., and Ulrich, J. (2015). Bw horizon in Holocene slope deposits (Kratzeburg, NE Germany) – dating and pedological characteristics. *E&G Quaternary Science Journal* **64,** 111–117.

Lahr, M. M., Rivera, F., Power, R. K., Mounier, A., Copsey, B., Crivellaro, F., Edung, J. E., Fernandez, J. M. M., Kiarie, C., Lawrence, J., Leakey, A., Mbua, E., Miller, H., Muigai, A., Mukhongo, D. M., Van Baelen, A., Wood, R., Schwenninger, J. L., Grün, R., Achyuthan, H., Wilshaw, A., and Foley, R. A. (2016). Inter-group violence among early Holocene hunter-gatherers of West Turkana, Kenya. *Nature* **529,** 394-398.

Lanckriet, S., Schwenninger, J.-L., Frankl, A., and Nyssen, J. (2015). The Late-Holocene geomorphic history of the Ethiopian Highlands: Supportive evidence from May Tsimble. *Catena* **135,** 290-303.

Leonard, S., and Nott, J. (2016). A Holocene fluvial archive of the Mulgrave River, Notheastern Australia: Influence of tropical cyclones and sediment delivery to the Great Barrier Reef. *Palaeogeography, Palaeoclimatology, Palaeoecology* **441, Part 4,** 845-853.

Li, D., Du, J., Ma, Y., and Xiao, A. (2015). Active faults and dip slip rates along the northern margins of the Huashan Mountain and Weinan loess tableland in the southeastern Weihe Graben, central China. *Journal of Asian Earth Sciences* **114,** 266-278.

Li, T., Wu, Y., Du, S., Huang, W., Hao, C., Guo, C., Zhang, M., and Fu, T. (2016). Geochemical characterization of a Holocene aeolian profile in the Zhongba area (southern Tibet, China) and its paleoclimatic implications. *Aeolian Research* **20,** 169-175.

Liu, B., Zhu, G., Zhai, M., Gu, C., and Liu, S. (2015). Quaternary faulting of the Jiangsu part of the Tan-Lu Fault Zone, East China: Evidence from field investigations and OSL dating. *Journal of Asian Earth Sciences* **114,** 89-102.

Liu, X.-J., Madsen, D. B., Liu, R., Sun, Y., and Wang, Y. (2016). Holocene lake level variations of Longmu Co, western Qinghai-Tibetan Plateau. *Environmental Earth Sciences* **75,** 1-14.

Liu, Y., Sun, Q., Thomas, I., Zhang, L., Finlayson, B., Zhang, W., Chen, J., and Chen, Z. (2015). Middle Holocene coastal environment and the rise of the Liangzhu City complex on the Yangtze delta, China. *Quaternary Research* **84,** 326-334.

Long, H., Fuchs, M., Yang, L., and Cheng, H. (2016). Abrupt sand-dune accumulation at the northeastern margin of the Tibetan Plateau challenges the wet MIS3a inferred from numerous lake-highstands. *Scientific Reports* **6,** 25820.

Lu, H., Xu, Y., Niu, Y., Wang, Z., Wang, H., Zhao, J., Zhang, W., and Zheng, X. (2016). Late Quaternary loess deposition in the southern Chaiwopu Basin of the northern Chinese Tian Shan foreland and its palaeoclimatic implications. *Boreas* **45,** 304-321.

Manaa, A. A., Jones, B. G., McGregor, H. V., Zhao, J.-x., and Price, D. M. (2016). Dating Quaternary raised coral terraces along the Saudi Arabian Red Sea coast. *Marine Geology* **374,** 59-72.

Margold, M., Jansen, J. D., Gurinov, A. L., Codilean, A. T., Fink, D., Preusser, F., Reznichenko, N. V., and Mifsud, C. (2016). Extensive glaciation in Transbaikalia, Siberia, at the Last Glacial Maximum. *Quaternary Science Reviews* **132,** 161-174.

Matmon, A., Elfassi, S., Hidy, A., Geller, Y., and Porat, N. (2016). Controls on aggradation and incision in the NE Negev, Israel, since the middle Pleistocene. *Geomorphology* **261,** 132-146.

May, S. M., Falvard, S., Norpoth, M., Pint, A., Brill, D., Engel, M., Scheffers, A., Dierick, M., Paris, R., Squire, P., and Brückner, H. (2016). A mid-Holocene candidate tsunami deposit from the NW Cape (Western Australia). *Sedimentary Geology* **332,** 40-50.

Meriç, E., Yokeş, M. B., Avşar, N., Kıyak, N. G., Öner, E., Nazik, A., Demirtaşlı, E., Dinçer, F., and Öztürk, M. Z. (2016). Did Amphistegina lobifera Larsen reach the Mediterranean via the Suez Canal? *Quaternary International* **401,** 91-98.

Moncel, M.-H., Despriée, J., Voinchet, P., Courcimault, G., Hardy, B., Bahain, J.-J., Puaud, S., Gallet, X., and Falguères, C. (2016). The Acheulean workshop of la Noira (France, 700 ka) in the European technological context. *Quaternary International* **393,** 112-136.

Morais, E. S. d., Santos, M. L. d., Cremon, É. H., and Stevaux, J. C. (2016). Floodplain evolution in a confluence zone: Paraná and Ivaí rivers, Brazil. *Geomorphology* **257,** 1-9.

Muñoz-Salinas, E., Castillo, M., Sanderson, D., Kinnaird, T., and Cruz-Zaragoza, E. (2016). Using three different approaches of OSL for the study of young fluvial sediments at the coastal plain of the Usumacinta–Grijalva River Basin, southern Mexico. *Earth Surface Processes and Landforms* **41,** 823-834.

Nicoll, K., and Keen-Zebert, A. (2016). Initial chronological determinations at an Archaic site discovered near Stockton, Utah. *Journal of Archaeological Science: Reports* **6,** 418-423.

Nordt, L., Bongino, J., Forman, S., Esker, D., and Benedict, A. (2015). Late Quaternary environments of the Waco Mammoth site, Texas USA. *Quaternary Research* **84,** 423-438.

Odriozola, C. P., Villalobos García, R., Burbidge, C. I., Boaventura, R., Sousa, A. C., Rodríguez-Ariza, O., Parrilla-Giraldez, R., Prudênçio, M. I., and Dias, M. I. (2016). Distribution and chronological framework for Iberian variscite mining and consumption at Pico Centeno, Encinasola, Spain. *Quaternary Research* **85,** 159-176.

Oliva, M., Antoniades, D., Giralt, S., Granados, I., Pla-Rabes, S., Toro, M., Liu, E. J., Sanjurjo, J., and Vieira, G. (2016). The Holocene deglaciation of the Byers Peninsula (Livingston Island, Antarctica) based on the dating of lake sedimentary records. *Geomorphology* **261,** 89-102.

Ollé, A., Vergès, J. M., Rodríguez-Álvarez, X. P., Cáceres, I., Angelucci, D. E., Vallverdú, J., Demuro, M., Arnold, L. J., Falguères, C., Bennàsar, M., López-García, J. M., Blain, H.-A., Bañuls-Cardona, S., Burjachs, F., Expósito, I., López-Polín, L., and López-Ortega, E. (2016). The Middle Pleistocene site of La Cansaladeta (Tarragona, Spain): Stratigraphic and archaeological succession. *Quaternary International* **393,** 137-157.

Ozcelik, M. (2015). Optically stimulated luminescence (OSL) dating of quartz grains within the sand dykes cutting the lacustrine deposits in the Burdur area (SW Turkey) and its tectonic interpretation. *Arabian Journal of Geosciences* **9,** 1-12.

Ozcelik, M. (2016). Evaluation of soft sediment deformation structures along the Fethiye-Burdur Fault Zone, SW Turkey. *Journal of Earth System Science* **125,** 343-358.

Ozturk, M. Z., Erginal, A. E., Kiyak, N. G., and Ozturk, T. (2016). Cement fabrics and optical luminescence ages of beachrock, North Cyprus: Implications for Holocene sea-level changes. *Quaternary International* **401,** 132-140.

Pagonis, V., Polymeris, G., and Kitis, G. (2015). On the effect of optical and isothermal treatments on luminescence signals from feldspars. *Radiation Measurements* **82,** 93-101.

Palamakumbura, R. N., Robertson, A. H. F., Kinnaird, T. C., and Sanderson, D. C. W. (2016). Sedimentary development and correlation of Late Quaternary terraces in the Kyrenia Range, northern Cyprus, using a combination of sedimentology and optical luminescence data. *International Journal of Earth Sciences* **105,** 439-462.

Peeters, J., Busschers, F. S., Stouthamer, E., Bosch, J. H. A., Van den Berg, M. W., Wallinga, J., Versendaal, A. J., Bunnik, F. P. M., and Middelkoop, H. (2016). Sedimentary architecture and chronostratigraphy of a late Quaternary incised-valley fill: A case study of the late Middle and Late Pleistocene Rhine system in the Netherlands. *Quaternary Science Reviews* **131, Part A,** 211-236.

Peng, J., and Pagonis, V. (2016). Simulating comprehensive kinetic models for quartz luminescence using the R program KMS. *Radiation Measurements* **86,** 63-70.

Polymeris, G. S., Kitis, G., Kiyak, N. G., Theodosoglou, E., Tsirliganis, N. C., Ertek, A., and Erginal, A. E. (2016). Dating fossil root cast (Black Sea coast, Turkey) using thermoluminescence: Implications for windblown drift of shelf carbonates during MIS 2. *Quaternary International* **401,** 184-193.

Portenga, E. W., and Bishop, P. (2016). Confirming geomorphological interpretations based on portable OSL reader data. *Earth Surface Processes and Landforms* **41,** 427-432.

Preoteasa, L., Vespremeanu-Stroe, A., Tătui, F., Zăinescu, F., Timar-Gabor, A., and Cîrdan, I. (2016). The evolution of an asymmetric deltaic lobe (Sf. Gheorghe, Danube) in association with cyclic development of the river-mouth bar: Long-term pattern and present adaptations to human-induced sediment depletion. *Geomorphology* **253,** 59-73.

Qiang, M., Jin, Y., Liu, X., Song, L., Li, H., Li, F., and Chen, F. (2016). Late Pleistocene and Holocene aeolian sedimentation in Gonghe Basin, northeastern Qinghai-Tibetan Plateau: Variability, processes, and climatic implications. *Quaternary Science Reviews* **132,** 57-73.

Rawat, N. S., Muthe, K. P., Dhabekar, B., Gaikwad, N. P., and Kulkarni, M. S. (2015). On the feasibility of multiple assessment of dose using CW-OSL technique in Al2O3:C. *Radiation Measurements* **82,** 74-82.

Ren, S., Song, C., and Li, J. (2016). Application of electron spin resonance (ESR) dating to ductile shearing: Examples from the Qinling orogenic belt, China. *Journal of Structural Geology* **85,** 12-17.

Richter, D., and Krbetschek, M. (2015). The age of the Lower Paleolithic occupation at Schöningen. *Journal of Human Evolution* **89,** 46-56.

Richter, D., Mittelstraß, D., Kreutzer, S., Pintaske, R., Dornich, K., and Fuchs, M. (2016). A new fully integrated X-ray irradiator system for dosimetric research. *Applied Radiation and Isotopes* **112,** 122-130.

Ritz, J. F., Avagyan, A., Mkrtchyan, M., Nazari, H., Blard, P. H., Karakhanian, A., Philip, H., Balescu, S., Mahan, S., Huot, S., Münch, P., and Lamothe, M. (2016). Active tectonics within the NW and SE extensions of the Pambak-Sevan-Syunik fault: Implications for the present geodynamics of Armenia. *Quaternary International* **395,** 61-78.

Ruszkiczay-Rüdiger, Z., Braucher, R., Novothny, A., Csillag, G., Fodor, L., Molnár, G., and Madarász, B. (2016). Tectonic and climatic control on terrace formation: Coupling in situ produced 10Be depth profiles and luminescence approach, Danube River, Hungary, Central Europe. *Quaternary Science Reviews* **131,** 127-147.

Sanjurjo-Sánchez, J., Gomez-Heras, M., Fort, R., Alvarez de Buergo, M., Izquierdo Benito, R., and Bru, M. A. (2016). Dating fires and estimating the temperature attained on stone surfaces. The case of Ciudad de Vascos (Spain). *Microchemical Journal* **127,** 247-255.

Schielein, P., Schellmann, G., Lomax, J., Preusser, F., and Fiebig, M. (2015). Chronostratigraphy of the Hochterrassen in the lower Lech valley (Northern Alpine Foreland). *E&G Quaternary Science Journal* **64,** 15-28.

Schildgen, T. F., Robinson, R. A. J., Savi, S., Phillips, W. M., Spencer, J. Q. G., Bookhagen, B., Scherler, D., Tofelde, S., Alonso, R. N., Kubik, P. W., Binnie, S. A., and Strecker, M. R. (2016). Landscape response to late Pleistocene climate change in NW Argentina: Sediment flux modulated by basin geometry and connectivity. *Journal of Geophysical Research F: Earth Surface* **121,** 392-414.

Shen, Z., and Lang, A. (2016). Quartz fast component opticallystimulated luminescence: Towards routine extraction for dating applications. *Radiation Measurements* **89,** 27-34.

Shen, Z., Törnqvist, T. E., Mauz, B., Chamberlain, E. L., Nijhuis, A. G., and Sandoval, L. (2015). Episodic overbank deposition as a dominant mechanism of floodplain and delta-plain aggradation. *Geology* **43,** 875-878.

Sivan, D., Greenbaum, N., Cohen-Seffer, R., Sisma-Ventura, G., Almogi-Labin, A., Porat, N., Melamed, Y., Boaretto, E., and Avnaim-Katav, S. (2016). Palaeo-environmental archive of groundwater–surface water interaction zone, the Kebara wetlands, Carmel coast, Israel. *Quaternary International* **396,** 138-149.

Smedley, R. K., Glasser, N. F., and Duller, G. A. T. (2016). Luminescence dating of glacial advances at Lago Buenos Aires (~46 °S), Patagonia. *Quaternary Science Reviews* **134,** 59-73.

Sun, X., Li, Y., Feng, X., Lu, C., Lu, H., Yi, S., Wang, S., and Wu, S.-Y. (2016). Pedostratigraphy of aeolian deposition near the Yunxian Man site on the Hanjiang River terraces, Yunxian Basin, central China. *Quaternary International* **400,** 187-194.

Tamura, T., Kodama, Y., Bateman, M. D., Saitoh, Y., Yamaguchi, N., and Matsumoto, D. (2016). Late Holocene aeolian sedimentation in the Tottori coastal dune field, Japan Sea, affected by the East Asian winter monsoon. *Quaternary International* **397,** 147-158.

Thomsen, K. J., Murray, A. S., Buylaert, J. P., Jain, M., Hansen, J. H., and Aubry, T. (2016). Testing single-grain quartz OSL methods using sediment samples with independent age control from the Bordes-Fitte rockshelter (Roches d'Abilly site, Central France). *Quaternary Geochronology* **31,** 77-96.

Tolksdorf, J. F., Turner, F., Nelle, O., Peters, S., and Brückner, H. (2015). Environmental development and local human impact in the Jeetzel valley (N Germany) since 10 ka BP as detected by geoarchaeological analyses in a coupled aeolian and lacustrine sediment archive at Soven. *E&G Quaternary Science Journal* **64,** 95-110.

Tripaldi, A., and Forman, S. L. (2016). Eolian depositional phases during the past 50 ka and inferred climate variability for the Pampean Sand Sea, western Pampas, Argentina. *Quaternary Science Reviews* **139,** 77-93.

Tsakalos, E., Christodoulakis, J., and Charalambous, L. (2016). The Dose Rate Calculator (DRc) for Luminescence and ESR Dating—a Java Application for Dose Rate and Age Determination. *Archaeometry* **58,** 347-352.

Tseng, C.-H., Lüthgens, C., Tsukamoto, S., Reimann, T., Frechen, M., and Böse, M. (2016). Late Pleistocene to Holocene alluvial tableland formation in an intra-mountainous basin in a tectonically active mountain belt — A case study in the Puli Basin, central Taiwan. *Quaternary Science Reviews* **132,** 26-39.

Tsukamoto, S., and Rades, E. F. (2016). Performance of pulsed OSL stimulation for minimising the feldspar signal contamination in quartz samples. *Radiation Measurements* **84,** 26-33.

Tudyka, K., and Bluszcz, A. (2016). A study on photomultiplier afterpulses in TL/OSL readers. *Radiation Measurements* **86,** 39-48.

van Aardt, A. C., Bousman, C. B., Brink, J. S., Brook, G. A., Jacobs, Z., du Preez, P. J., Rossouw, L., and Scott, L. (2015). First chronological, Palaeoenvironmental, and archaeological data from the Baden-Baden fossil spring complex in the western Free State, South Africa. *In* "Changing Climates, Ecosystems and Environments within Arid Southern Africa and Adjoining Regions." pp. 117-152. Palaeoecology of Africa. CRC Press.

van den Bergh, G. D., Li, B., Brumm, A., Grün, R., Yurnaldi, D., Moore, M. W., Kurniawan, I., Setiawan, R., Aziz, F., Roberts, R. G., Suyono, Storey, M., Setiabudi, E., and Morwood, M. J. (2016). Earliest hominin occupation of Sulawesi, Indonesia. *Nature* **529,** 208-211.

Voinchet, P., Brulhet, J., Cojan, I., Bahain, J.-J., and Falguères, C. (2015). Datation ESR des terrasses alluviales pléistocènes de la vallée de l'Aube : premiers résultats. *Quaternaire* **26,** 185-193.

Wacha, L., Vlahović, I., Tsukamoto, S., Kovačić, M., Hasan, O., and Pavelić, D. (2016). The chronostratigraphy of the latest Middle Pleistocene aeolian and alluvial activity on the Island of Hvar, eastern Adriatic, Croatia. *Boreas* **45,** 152-164.

Weiss, M. (2015). Stone tool analysis and context of a new late Middle Paleolithic site in western central Europe – Pouch-Terrassenpfeiler, Ldkr. Anhalt-Bitterfeld, Germany. *In* "Quartär: Internationales Jahrbuch zur Eiszeitalter- und Steinzeitforschung / International Yearbook for Ice Age and Stone Age Research." (W. Müller, S. Costamagno, B. V. Eriksen, T. Hauck, Z. Mester, L. Moreau, D. Richter, I. Schmidt, M. Street, E. Turner, and G.-C. Weniger, Eds.), pp. 23-62. Verlag Marie Leidorf, Rahden.

Williams, M. A. J., Duller, G. A. T., Williams, F. M., Woodward, J. C., Macklin, M. G., El Tom, O. A. M., Munro, R. N., El Hajaz, Y., and Barrows, T. T. (2015). Causal links between Nile floods and eastern Mediterranean sapropel formation during the past 125 kyr confirmed by OSL and radiocarbon dating of Blue and White Nile sediments. *Quaternary Science Reviews* **130,** 89-108.

Wolf, D., Baumgart, P., Meszner, S., Fülling, A., Haubold, F., Sahakyan, L., Meliksetian, K., and Faust, D. (2016). Loess in Armenia – stratigraphic findings and palaeoenvironmental indications. *Proceedings of the Geologists' Association* **127,** 29-39.

Wu, C., Wu, G., Shen, J., Dai, X., Chen, J., and Song, H. (2016). Late Quaternary tectonic activity and crustal shortening rate of the Bogda mountain area, eastern Tian Shan, China. *Journal of Asian Earth Sciences* **119,** 20-29.

Yang, X., Forman, S., Hu, F., Zhang, D., Liu, Z., and Li, H. (2016). Initial insights into the age and origin of the Kubuqi sand sea of northern China. *Geomorphology* **259,** 30-39.

Yu, K., Hartmann, K., Nottebaum, V., Stauch, G., Lu, H., Zeeden, C., Yi, S., Wünnemann, B., and Lehmkuhl, F. (2016). Discriminating sediment archives and sedimentary processes in the arid endorheic Ejina Basin, NW China using a robust geochemical approach. *Journal of Asian Earth Sciences* **119,** 128-144.

Zabcı, C., Sançar, T., Akyüz, H. S., and Kıyak, N. G. (2015). Spatial slip behavior of large strike-slip fault belts: Implications for the Holocene slip rates of the eastern termination of the North Anatolian Fault, Turkey. *Journal of Geophysical Research: Solid Earth* **120,** 8591-8609.

Zeng, L., Lu, H., Yi, S., Li, Y., Lv, A., Zhang, W., Xu, Z., Wu, H., Feng, H., and Cui, M. (2016). New magnetostratigraphic and pedostratigraphic investigations of loess deposits in north-east China and their implications for regional environmental change during the Mid-Pleistocene climatic transition. *Journal of Quaternary Science* **31,** 20-32.

Zhang, J., Tsukamoto, S., Jia, Y., and Frechen, M. (2016). Lake level reconstruction of Huangqihai Lake in northern China since MIS 3 based on pulsed optically stimulated luminescence dating. *Journal of Quaternary Science* **31,** 225-238.

Zhao, H., Sheng, Y., Li, B., and Fan, Y. (2016). Holocene environment changes around the Sara Us River, northern China, revealed by optical dating of lacustrine–aeolian sediments. *Journal of Asian Earth Sciences* **120,** 184-191.

Zhao, X., Huang, C. C., Pang, J., Zha, X., Guo, Y., and Hu, G. (2016). Holocene climatic events recorded in palaeoflood slackwater deposits along the middle Yiluohe River valley, middle Yellow River basin, China. *Journal of Asian Earth Sciences* **123,** 85-94.

Zhu, B. Q. (2016). Atmospheric significance of aeolian salts in the sandy deserts of northwestern China. *Solid Earth* **7,** 191-203.

Zieliński, P., Sokołowski, R. J., Woronko, B., Fedorowicz, S., Jankowski, M., and Standzikowski, K. (2016). Sandy deposition in a small dry valley in the periglacial zone of the Last Glacial Maximum: A case study from the Józefów site, SE Poland. *Quaternary International* **399,** 58-71.

Zink, A., Richardin, P., Gandolfo, N., and Rante, R. (2015). Le Grand Khorasan: Datation par des méthodes physico-chimiques (carbone 14 et luminescence). *In* "Greater Khorasan: History, Geography, Archaeology and Material Culture." pp. 161-176.

Conference Announcements: German LED 2016

German Luminescence and ESR Meeting

4.-6.11.2016, Emmendingen

The meeting is this year organised by the Chair in Sedimentology of Albert-Ludwig-Universität Freiburg. Venue will be the hotel Windenreuther Hof in Emmendingen (http://hotel-windenreuter-hof.de/). The hotel is located in a beautiful position in the transition from the Black Forest towards the Upper Rhine Graben. We will all stay together in the hotel where the meeting will take place. The meeting starts on Friday at ca. 14:00, and closes Sunday ca. 12:00.

The all-inclusive registration fee comprises the conference costs, accommodation and meals. It depends on the room category (further information is found on the registration form):

Single room:	EUR 240,- (payment until 15.09., afterwards EUR 270,-)
Two bed room:	EUR 200,- (payment until 15.09., afterwards EUR 230,-)
Three bed room:	EUR 185,- (payment until 15.09., afterwards EUR 215,-)

Please visits the webpage: https://www.sedimentologie.uni-freiburg.de/german-led-2016

The regular registration deadline ends **15.09.2016**. Afterwards we have to add a late registration addition of EUR 30,-. Please send the filled-out registration form as well as all requests and suggestions regarding the meeting to the following email address: led2016@geologie.uni-freiburg.de

Best wishes and see you soon,
Frank Preusser und Team

Conference Announcements: LED 15

Dear Colleagues

Rhodes University, South Africa, is pleased to announce the **15th International Conference on Luminescence and Electron Spin Resonance to be held in Cape Town, South Africa, in September 2017**. This is the first time the conference will have been held in Africa and the local organising committee is looking forward to welcoming delegates to Cape Town. The conference topics will include but are not limited to the following:

- Basic physical processes and materials' characteristics
- Instrumentation and procedures
- Advances in equivalent dose determination
- Advances in dose rate determination
- Innovative dating approaches
- Applications in Earth and Planetary Sciences
- Applications in Archaeology
- ESR: advances and applications

The conference website is at www.led2017.com.

Makaiko Chithambo

Chairman, Local Organising Committee

Ancient TL

ISSN 0735-1348

Aims and Scope

Ancient TL is a journal devoted to Luminescence dating, Electron Spin Resonance (ESR) dating, and related techniques. It aims to publish papers dealing with experimental and theoretical results in this field, with a minimum of delay between submission and publication. Ancient TL also publishes a current bibliography, thesis abstracts, letters, and miscellaneous information, e.g., announcements for meetings.

Frequency

Two issues per annum in June and December

Submission of articles to Ancient TL

Ancient TL has a reviewing system in which direct dialogue is encouraged between reviewers and authors. For instructions to authors and information on how to submit to Ancient TL, please visit the website at:
http://www.ecu.edu/cs-cas/physics/ancient-timeline/ancient-tl1.cfm

Journal Enquiries

For enquiries please contact the editor:
Regina DeWitt, Department of Physics, East Carolina University, Howell Science Complex, 1000 E. 5th Street, Greenville, NC 27858, USA; Tel: +252-328-4980; Fax: +252-328-0753 (dewittr@ecu.edu)

Subscriptions to Ancient TL

Ancient TL Vol. 32 No.2 December 2014 was the last issue to be published in print. Past and current issues are available for download free of charge from the Ancient TL website:
http://www.ecu.edu/cs-cas/physics/ancient-timeline/ancient-tl5.cfm